CHALMERS
UNIVERSITY OF TECHNOLOGY

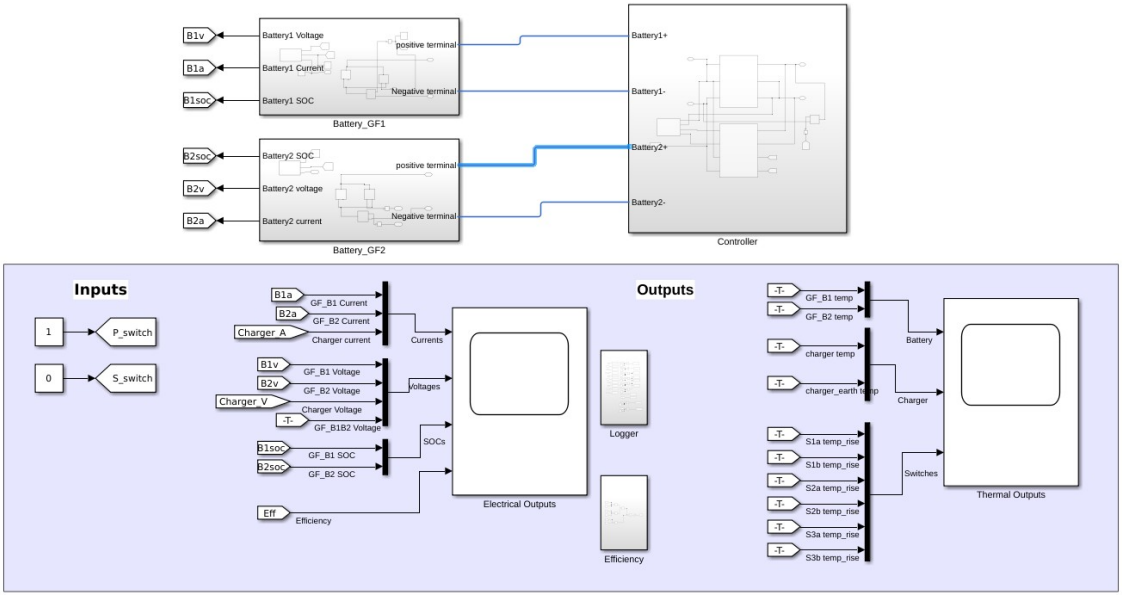

Modelling and Comparative Analysis of Switchable Battery Configurations for Dual Voltage Charging in Electric Vehicles

Master of Science Thesis in Sustainable Energy Systems

ABHILASH VENKAT NARAYANAN
IFEANYICHUKWU OREOLUWA AZOGU

DEPARTMENT OF ELECTRICAL ENGINEERING
CHALMERS UNIVERSITY OF TECHNOLOGY
Gothenburg, Sweden 2025
www.chalmers.se

Master of Science Thesis 2025

Modelling and Comparative Analysis of Switchable Battery Configurations for Dual Voltage Charging in Electric Vehicles

ABHILASH VENKAT NARAYANAN
IFEANYICHUKWU OREOLUWA AZOGU

CHALMERS
UNIVERSITY OF TECHNOLOGY

Department of Electrical Engineering
Division of Electric Power Engineering
Chalmers University of Technology
Gothenburg, Sweden 2025

Modelling and Comparative Analysis of Switchable Battery Configurations for Dual Voltage Charging in Electric Vehicles
ABHILASH VENKAT NARAYANAN
IFEANYICHUKWU OREOLUWA AZOGU

Supervisor: Filipe Ribeiro Magalhães, Volvo Cars
Examiner: Thorbjörn Thringer, Department of Electrical Engineering

Master of Science Thesis 2025
Department of Electrical Engineering
Division of Electric Power Engineering
Chalmers University of Technology
SE-412 96 Gothenburg
Telephone +46 31 772 1000

Cover: Matlab Simulink model of modular battery system.

Typeset in LaTeX
Printed by Chalmers Reproservice
Gothenburg, Sweden 2025

Modelling and Comparative Analysis of Switchable Battery Configurations for Dual Voltage Charging in Electric Vehicles
ABHILASH VENKAT NARAYANAN
IFEANYICHUKWU OREOLUWA AZOGU
Department of Electrical Engineering
Chalmers University of Technology

Abstract

This thesis explores and evaluates two electric vehicle (EV) battery architectures: an existing 800V single battery system using inverter-based 400V charging referred to as the DC boost system, and a proposed dual 400V battery system that allows series-parallel switching for direct 400V charging, referred to as the Greenfield system. The main aim is to identify energy losses in these systems and investigate architectural and material solutions to enhance efficiency, thermal performance, reliability, and cost-effectiveness.

A MATLAB Simulink model was created to simulate energy flows, battery behaviour, and thermal dynamics under a variety of charging conditions, spanning from realistic to sensitivity-driven scenarios. Battery balancing mechanisms were incorporated to evaluate system performance when SOC mismatches occur. Although both systems achieve comparable efficiencies during 400V charging, the proposed architecture shows lower energy losses, improved thermal performance and longer component lifespan due to decreased current stress and the removal of voltage boosting with the inverter. Furthermore, the possibility of replacing aluminium with copper busbars was studied, revealing lower thermal peaks while retaining electrical performance.

Overall, the findings indicate that even though the energy efficiency differences between the two systems are slight, the Greenfield system provides significant benefits in thermal stability and component durability, particularly during high-current operation. These results highlight the trade-offs involved in system complexity, material choice, and long-term performance in the design of EV battery systems.

Keywords: Modular Battery Systems, Battery Disconnect Unit, Electric Vehicles, Energy Efficiency, High Voltage Batteries, SIMULINK Modelling, Series-Parallel Configuration, Voltage Boosting, Busbars.

Acknowledgements

This work has been carried out at Volvo Cars, in collaboration with the Department of Electrical Engineering, Chalmers University of Technology. The research was conducted as part of the requirements for the Sustainable Energy Systems Master's Program at Chalmers University of Technology.

We would like to extend our gratitude to our supervisor, Filipe Ribeiro Magalhães, for his invaluable guidance, constructive feedback and continuous support throughout our thesis journey. Their expertise and encouragement has played a vital role in shaping our research and deepening our understanding of the subject.

We also acknowledge the support of our examiner, Torbjörn Thiringer, whose insights have contributed to refining the scope and methodology of this work. Additionally, we are grateful to Chalmers University of Technology for providing us with the resources, knowledge, and opportunities necessary to undertake this research.

A heartfelt thank you to our families and friends for their unwavering suppport, patience, and encouragement. Your belief in us has been a source of strength and motivation, helping us navigate the challenges of this academic endeavour.

Finally, we acknowledge and appreciate everyone who has contributed, directly or indirectly, to the successful completion of this thesis, including the countless amount of coffee that fuelled our long nights and kept us typing. All the support has been truly invaluable.

Abhilash Venkat Narayanan
Ifeanyichukwu Oreoluwa Azogu
Göteborg, Sweden, 2025

List of Acronyms

Below is the list of acronyms that have been used throughout this thesis listed in alphabetical order:

AC	Alternating current
BDU	Battery Disconnection Unit
BMS	Battery Management System
DC	Direct Current
EVs	Electric Vehicles
EOL	End of Life
FPMH	Failures Per Million Hours
GM	General Motors
IGBT	Insulated Gate Bipolar Transisitor
MOSFET	Metal-Oxide-Semiconductor Field-Effect Transistor
MIS	Months in Service
OBC	On-Board Charger
PD	Partial Discharge
PDIV	Partial Discharge Inception Voltage
PPM	Parts per Million
PCB	Printed Circuit Board
PWM	Pulse Width Modulation
RC	Resistance Capacitance
SOC	State Of Charge

Nomenclature

Below is the nomenclature of indices, sets, parameters, and variables that have been used throughout this thesis.

Indices

i	Indices for currents and voltages in the system
t	Index for time step

Parameters

R_{on}	On-state resistance of the conductor
f_{sw}	Switching frequency of the switch
t_r	Rise/Fall time of the switch
R_0	Nominal resistance at reference temperature
T_0	Reference temperature
α	Temperature coefficient
t_c	Thermal time constant
K_d	Dissipation factor

Variables

P_i	Calculated Power/Power loss in the system
I_i	Current flowing through a conductor in the system
V_i	Voltage across two terminals in the system
T	Final Temperature at the end of simulation
Q	Net heat flow through a conductor
η	System Efficiency

Contents

1
Introduction

1.1 Background

The increasing electrification of the automotive industry has led to significant advancements in battery technology, with higher energy density and efficiency becoming key priorities. Although energy losses within battery systems remain a critical challenge, affecting vehicle range, charging efficiency, and thermal performance.

This thesis, conducted in collaboration with Volvo Cars, aims to analyze and compare two different battery system architectures for electric vehicles (EVs) in terms of energy efficiency, safety, complexity, cost, and feasibility. The study will focus on:

1. DC boost System – A Single Battery Architecture with Voltage Boosting, where an 800V battery system uses the vehicle's motor, inverter and the DC-DC converter to boost the voltage during charging from a 400V AC grid connection. The system bypasses the motor, inverter and the DC-DC converter when connected to DC fast charging. Although this approach enables high-power charging, it introduces conversion losses and additional thermal load.
2. Greenfield System – A Modular Battery Architecture with Series-Parallel Configuration, where two 400V battery modules can be connected in series (for 800V operation) or parallel (for 400V charging) using relays, eliminating the need for the motor, inverter and DC-DC converter. This configuration has the potential to improve efficiency and energy utilization, but it introduces challenges in component integration and system reliability.

Several studies have analyzed the architectures of the battery system for EVs, focusing on energy efficiency, thermal effects, and charging strategies. Research on single 800V battery systems has demonstrated their effectiveness in supporting fast charging but also highlighted conversion inefficiencies associated with motor-inverter-assisted voltage boost. Investigations of modular battery configurations (in this case, two 400V batteries in series) suggest that direct DC charging can improve efficiency, although challenges remain in balancing charge distribution and managing internal losses [1].

In modern EVs, inverter based voltage boosting is the dominant method used to achieve 800V charging from an AC source. This approach leverages an existing traction inverter to step up the onboard AC voltage, with the assistance of the traction motor, reducing hardware redundancy and aligning with industry trends favouring compact, integrated systems [2][3]. In contrast, the switchable battery architecture, which dynamically alternates between series and parallel configurations, are less common due to challenges in control complexity, contactor reliability and

safety under high voltage conditions[4][5]. Despite their potential to eliminate voltage conversion and reduced conduction losses, real world applications seems limited. This study explores a comparative study between the two architectures, assessing not only efficiency and thermal performance, but also their impact on system reliability and cost. While prior research have focused on the electrical performance of individual systems, a holistic evaluation covering performance and practical implementation remains sparse, highlighting the relevance and novelty of this work.

1.2 Purpose

The primary objective of this thesis is to determine where major energy losses occur within the battery system and propose countermeasures to improve efficiency. Specifically, the study will:

1. Compare energy losses in the DC boost system (single 800V battery with motor inverter-assisted AC charging) and the Greenfield system (two 400V batteries in series with direct DC charging) under different charging scenarios.
2. Analyse the impact of thermal management on system efficiency and identify how heat dissipation affects overall performance.
3. Assess system complexity, safety, and financial feasibility between both architectures, considering manufacturing constraints and operational risks.
4. Identify potential design improvements to minimize energy losses in the existing system, with a focus on optimizing charging strategies and balancing techniques.

1.3 Research Questions

To achieve these objectives, the study will address the following key research questions:

- Where do the primary energy losses occur in each system during charging?
- How does each system handle thermal management and what are the associated losses?
- Which system presents greater safety risks and how can they be mitigated?
- What are the cost implications of using modular battery configurations vs. traditional single-battery architectures?
- How complex is each system in terms of design and control algorithms?
- What improvements can be made to reduce energy losses in the DC boost system?

1.4 Limitations

This study is subject to the following limitations:
The analysis is limited to the battery system boundary between the Battery Disconnection Unit (BDU) and the charging station (DC fast charging and home charging). Other vehicle subsystems (e.g., drivetrain, power electronics beyond the BDU) are

not considered. Due to proprietary restrictions, physical validation may be limited and analysis will primarily rely on simulation-based experiments rather than real-world testing. The study assumes standard 400V and 800V charging infrastructure without considering ultra-fast charging technologies exceeding 1000V. Moreover, an exhaustive examination of the DC booster cannot be conducted; therefore, the presumed losses in the system was provided as data and not measured.

By addressing these questions and constraints, this research aims to provide quantitative insights into the performance, feasibility, and optimization potential of both battery architectures, supporting future advancements in EV battery system design.

2

Theory

2.1 Introduction to theoretical framework

The implementation of dynamic battery switching systems in electric vehicles plays a critical role in optimising performance, efficiency, and charging stability. This section presents the theoretical foundation relevant to the study, focusing on battery configurations, switching mechanisms, component losses, control strategies, and their impact.

2.2 Battery architecture and switching mechanisms

Battery packs in EVs are configured in either series or parallel to achieve desired voltage and current levels. The series connection increases voltage while keeping current constant, usually done to extend the vehicle's range and used in high-voltage applications like DC fast charging. Parallel connections increase current while maintaining voltage, commonly employed for balancing power distribution and enhancing battery capacity. In hybrid configurations, some battery systems employ a combination of series and parallel switching to dynamically adapt to different operating conditions. The concept of reconfigurable battery packs, where modules are switched between series and parallel modes for efficient propulsion and charging, has been demonstrated in GM's Ultium platform [6].

Battery switching systems enable dynamic reconfiguration of battery packs to accommodate different operational needs but these dynamic reconfigurations introduce transient voltage changes that can lead to current spikes, energy losses, and temperature variations in the battery pack, which must be strategically managed to ensure long-term performance and safety. These can be achieved by either Mechanical Switches (Contactors) that physically connect and disconnect electrical circuits but have limitations in speed and durability or Solid-state Switches(MOSFETs) that provide fast and reliable switching with minimal losses but are not physically isolated and require complex strategies. Both come with a set of challenges that include minimizing switching losses, ensuring reliability, and maintaining thermal stability during high switching periods [7]. This study will utilize electro-mechanical contactors as solid state switches cannot provide full galvanic isolation which doesn't align the ISO26262 standard.

2.3 Simulation and Modelling of Battery Switching

Simulation software is essential for analysing and visualising the behaviour of dynamic battery switching systems. Electrical circuit modelling allows for in-depth evaluation of voltage and current variations under different switching conditions. In this investigation, MATLAB Simulink is the preferred software. Dynamic reconfiguration visualization is implemented to provide real-time monitoring of battery switching and SOC updates, thermal analysis of the system is achieved using thermo-electrical blocks in the Simulink environment. Additionally, validation through existing studies is crucial for comparing simulation results with real-world data to assess model accuracy and in optimizing battery switching strategies effectively.

2.4 Losses in the System

Based on the system architecture and proposed model, it is hypothesized that the most significant sources of energy loss arise from individual components and battery module balancing operations.

Ohmic losses are expected to dominate during high-current charging and discharging. These losses originate from the internal resistance of battery cells, interconnects, busbars, and contactors, and are proportional to the square of the current flowing through them. In high-voltage systems, such as the 800V configuration under study, it is anticipated these losses will be especially pronounced during fast charging and high-power discharge events.

2.4.1 Losses in Electromechanical Contactors

Electromechanical contactors are electricity-controlled switching devices, utilizing an electromagnetic coil to either open or close a collection of mechanical contacts, thus enabling or disabling electrical pathways. In EVs, contactors play a crucial role in connecting or disconnecting high-voltage components such as battery packs, inverters, and chargers. Their capacity to manage large currents is essential for both regular operations and protection against faults. Though these devices are robust and simple, they are associated with power losses and safety risks.

When contactors are closed, the contacts carry current with minimal resistance, conduction losses are more influenced by the square of the current. These losses can increase over time due to deterioration from oxidation, ageing, or micro-welding of contacts[2][8]. Operating under load may cause arcing, particularly during high in-rush currents, leading to erosion, pitting, or welding of the contacts, which increases contact resistance and heat generation. Continuous arcing degrades the contact surface, shortening electrical life and heightening the likelihood of contactor malfunction [2]. This is a primary cause of reduced contactor lifespan in high voltage applications [8]. Manufacturers specify contactors' life spans in terms of mechanical (no load) and electrical (under load) operations, typically from 100,000 to 1,000,000 cycles for mechanical, and from 10,000 to 100,000 cycles for electrical life, depending

on load and arc suppression strategies [9]. Frequent switching, high load currents, and temperature changes aggravate degradation [10]. Potential failure modes include welded contacts that do not open, chattering due to unstable contact, and delayed actuation from coil wear or deterioration. Solutions to these include using dual contactors for redundancy, incorporating pre-charge circuits, and implementing contact health monitoring techniques [2] [10].

2.4.2 Losses in inverters with boost functionality

In EVs, inverters play a significant role in converting DC to AC for motor drive during propulsion, and conversely, convert AC to DC during regenerative braking or AC fast charging. Some inverters also have boost functionality, enabling them to step up incoming AC voltage or adapt to varying charging or drive conditions, making them versatile for both driving and charging.[11]

One of the most significant losses in inverters is the switching losses, which occur during the transition period of power semiconductors (MOSFETs or IGBTs) when both voltage and current overlap. These losses are directly proportional to the switching frequency and the switching time of the devices [12]. High switching frequency is advantageous for compact passive components, but increases switching losses unless mitigated through advanced topologies or wide-gap semiconductors.

Additionally, conduction losses arise during the on-state of the semiconductor switches. For MOSFETs, this is attributed to their drain-source on-resistance, while IGBTs experience losses due to voltage drop. Conduction losses increase with current and operating temperature, making them critical during high-power charging [13].

Passive components like capacitors and inductors also contribute to losses. Inductor losses include core losses due to hysteresis and eddy current, as well as copper losses due to winding resistance. Capacitors have power dissipation through their equivalent series resistance, especially at higher ripple currents [14]. There are other losses like diode rectification losses, where the boost diode's forward voltage drop and recovery current contribute to thermal loss and voltage overshoots. To overcome this, synchronous rectification can be utilized, which replaces the diode with a controlled MOSFET, improving efficiency but increasing complexity [15]. Minor losses from the control circuitry like gate drivers, PWM controllers, and voltage feedback systems introduce minor parasitic losses, which add to the total system overhead.

Thermal management and PCB layout also contribute to loss behavior. Poor heat dissipation raises junction temperatures, increasing both conduction and switching losses, while excessive parasitic inductance due to poor PCB layout can cause electromagnetic interference and voltage spikes [12]. The Greenfield system, which allows switching between battery configurations, avoids using a inverter to increase the voltage from 400V to 800V when charging at 400V stations. This simplification enhances the system's overall efficiency by reducing the complexity and number of components in the pathway from charger to the battery pack.

2.4.3 Losses in Busbars

In high voltage EV architectures, busbars serve as the primary medium in transferring power between subsystems like battery packs and inverters. While they offer mechanical robustness and improved thermal handling compared to cables, they are not completely lossless.

The most prominent loss in busbars is the resistive or ohmic loss, caused due to the material resistance of the busbar. Although they are manufactured using low resistivity materials like copper and aluminium, their length, cross-section, and operating temperature influence the total resistance. Higher currents during fast charging can lead to higher ohmic losses [16]. In addition to ohmic losses, skin effect becomes significant at higher frequencies, especially in systems with fast switching converters. This causes current to concentrate near the surface of the busbar, effectively increasing the AC resistance of the busbar. This results in higher conduction losses compared to DC operation, particularly when operated with high ripple components from switching power electronics [17].

Eddy current losses also are significant when alternating magnetic fields induce circular currents within the conductive layers of the busbar. These losses increase with frequency and are significant in laminated or multi-layer busbars without adequate insulation between the layers [18]. Thermal losses due to resistive heating increase the busbar temperature, which further increases the busbar resistance, as it has a positive temperature coefficient of resistivity. Inadequate thermal management can also lead to insulation degradation and increased safety risks. Furthermore, joint and contact losses at interfaces, such as between busbar and contactor or busbar to terminal connections, introduce additional resistance and localized heating. These are affected by mechanical stress, oxidation, surface roughness, or loosening over time [19].

To mitigate these losses, some design strategies include an increased cross-sectional area, use of laminated busbars to minimize eddy currents, and application of silver or tin plating to reduce contact resistance. Some systems employ liquid cooling to actively manage thermal loads and maintain low resistance values under continuous operation [16][19].

2.5 Equations

To compare the efficiency figures generated by the model with the existing architecture, losses are also analytically computed using existing equations.

2.5.1 Conduction losses

The power loss in a conductor during conduction is given by

$$P_c = I_c^2 \, R_{on} \tag{2.1}$$

where P_c is the conduction losses in the conductor, I_c is the current flowing through the conductor, and R_on is the on-state resistance of the conductor.

2.5.2 Temperature rise in busbars

The temperature rise in busbars is calculated in the Simulink environment using the expression

$$R(T) = R_0 \cdot (1 + \alpha \cdot (T - T_0)) \tag{2.2}$$

where R_0 is the nominal resistance at reference temperature, T_0 is the reference temperature, and α is the temperature coefficient.
The temperature T is governed by the relation

$$K_d \cdot t_c \cdot \frac{dT}{dt} = Q + I_b^2 \cdot R(T) \tag{2.3}$$

where Q is the net heat flow into the busbar, I_b is the current flowing through the busbar, t_c is the thermal time constant, and K_d is the dissipation factor.

2.5.3 Power

The power is calculated using

$$P = V \times I \tag{2.4}$$

where P is the power, V is the voltage across the terminals, and I is the current passing through.

2.5.4 Losses

The system losses is calculated by

$$Losses = P_\mathrm{in} - P_\mathrm{out} \tag{2.5}$$

where Losses is the system Losses, P_{out} is the power going into the batteries during charging, and P_{in} is the power into the system from the charger.

2.5.5 Effect of Voltage Boosting

The temperature rise in the winding of the motor is estimated using the expression

$$\Delta T = I^2 R \cdot \eta_\mathrm{loss} + f_\mathrm{sw} \cdot C_\mathrm{core} \tag{2.6}$$

where I is the charging current, f_sw is switching frequency, and C_core is core loss coefficient.
Relative dV/dt Stress in the system is estimated using

$$\text{Relative dV/dt Stress} = \frac{\text{Peak dV/dt during Boosting}}{\text{Peak dV/dt during Normal Drive}} \tag{2.7}$$

where $\frac{dV}{dt}$ is the voltage rise rate during switching.
Partial Discharge (PD) Risk is estimated using the expression

$$\text{PD Risk} \propto \frac{T_\mathrm{winding} \cdot \frac{dV}{dt}}{\mathrm{PDIV}_\mathrm{initial}} \tag{2.8}$$

where T_winding is the stator winding temperature, $\frac{dV}{dt}$ is the voltage rise rate during switching, and $\mathrm{PDIV}_\mathrm{initial}$ is the initial partial discharge inception voltage of the motor insulation system.

3
Case Set-up

3.1 System Overview

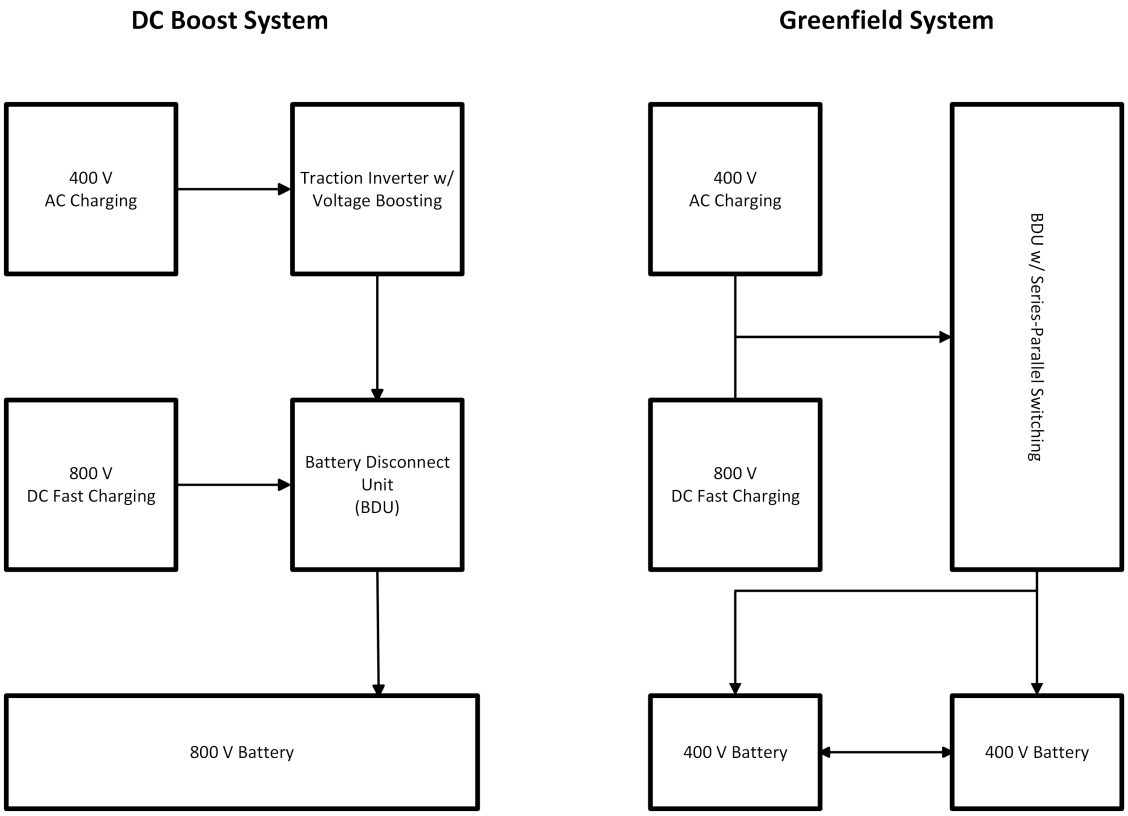

Figure 3.1: Simplified overview of DC boost and Greenfield System

Fig. 3.1 shows a simplified comparison between the DC boost and Greenfield system architectures. The DC boost system uses a single 800 V battery and relies on a traction inverter to boost 400 V AC charging up to 800 V, with both AC and DC fast charging routed through a Battery Disconnect Unit (BDU). The BDU serves as the primary safety and switching interface between the high-voltage battery and the rest of the electric vehicle powertrain. The Greenfield system reconfigures the single battery into two 400 V battery packs and uses a BDU with series-parallel switching. This allows the batteries to connect in series for 800V DC fast charging and in parallel for 400V AC charging, eliminating the need for inverter-based boosting.

The setup decouples AC charging from the traction system and offers a more flexible energy path.

In the DC boost system, the BDU includes main positive and negative contactors, a dedicated booster contactor to support voltage boosting during charging from a 400 V grid, and DC charging contactors for both positive and negative terminals as shown in Fig. 3.2.

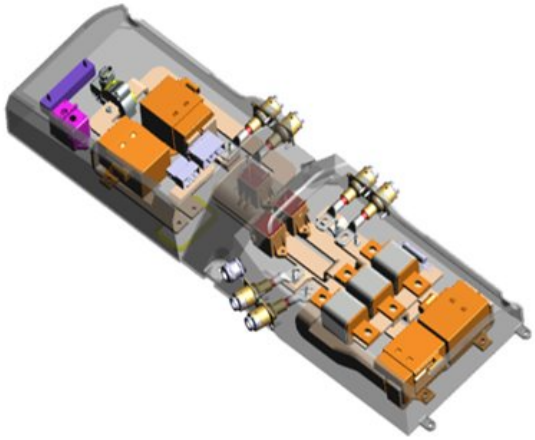

Figure 3.2: A Battery Disconnect Unit

It is compatible with both 400V and 800V charging, enabling adaptable charging. This can be achieved by employing the motor and inverter to perform 400V charging while boosting the voltage to 800V.

Boost-capable inverters for 800V battery charging via a 400V DC input require that the OBC boosts the voltage before supplying it to the battery as illustrated in Fig. 3.3.

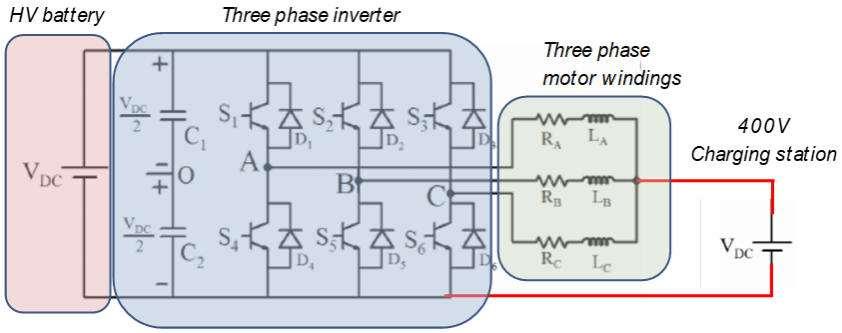

Figure 3.3: Voltage Boosting via EV Traction Motor

The oversized inverter boosts the voltage by routing power through the three-phase motor windings. While this technique enables compatibility with low-voltage chargers, it introduces an additional conversion stage, increasing energy losses and thermal stress on both the inverter and motor[20]. This complexity not only reduces overall charging efficiency but also imposes lifetime and derating constraints on the power

electronics. In contrast, switchable systems such as the proposed configuration support direct 400V charging in parallel mode, eliminating the boost stage and reducing component stress.

The reliability motivations for the Greenfield design can be traced to weaknesses in conventional EV battery systems. Fig. 3.4 highlights the primary reliability concerns that motivated the Greenfield design.

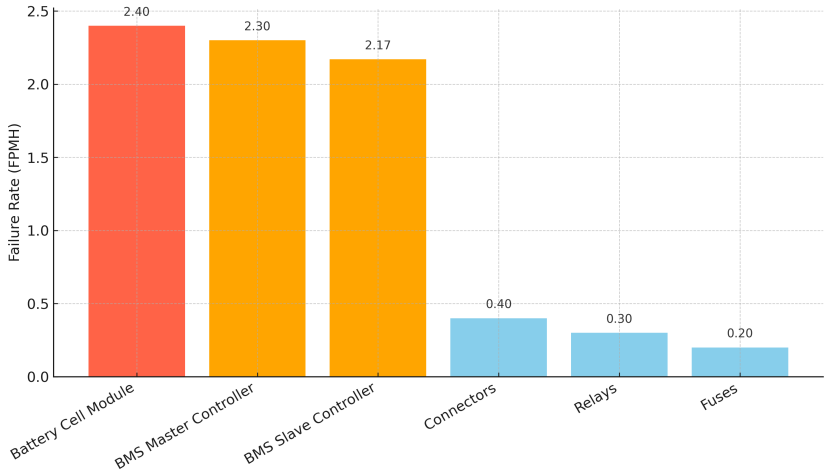

Figure 3.4: Select Components' failure rates as reported by Shu et al. [21]

These elements dominate system failure statistics, while ancillary components such as connectors, relays, and fuses maintain much lower rates, typically below 0.5 failures per million hours (FPMH). The proposed architecture seeks to mitigate stress on these critical components by simplifying the power flow and eliminating boost-stage complexity.

While the voltage boosting approach is effective in reducing hardware, Ji et al reported this exposes the motor insulation system to electrical and thermal stresses summarized in Fig. 3.5.

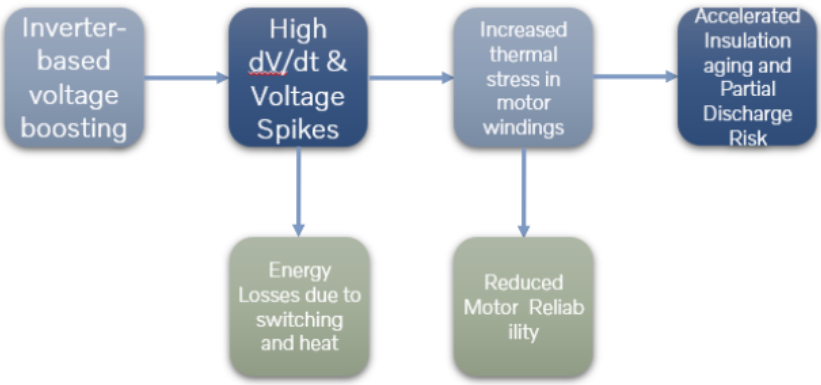

Figure 3.5: Effect of voltage boosting on the traction motor as reported by Ji et al. [22]

This insight underpins the proposed system architecture by simplifying or removing high-risk components (i.e. the oversized inverter and related parts in the BDU assembly) and reducing stress on the BMS. The design aims to dramatically improve overall reliability. In essence, every component in the power supply chain can affect system dependability [21], so the System Overview highlights a strategy of minimizing the count and complexity of components that historically dominate failure statistics.

3.1.1 Proposed Switching based Architecture

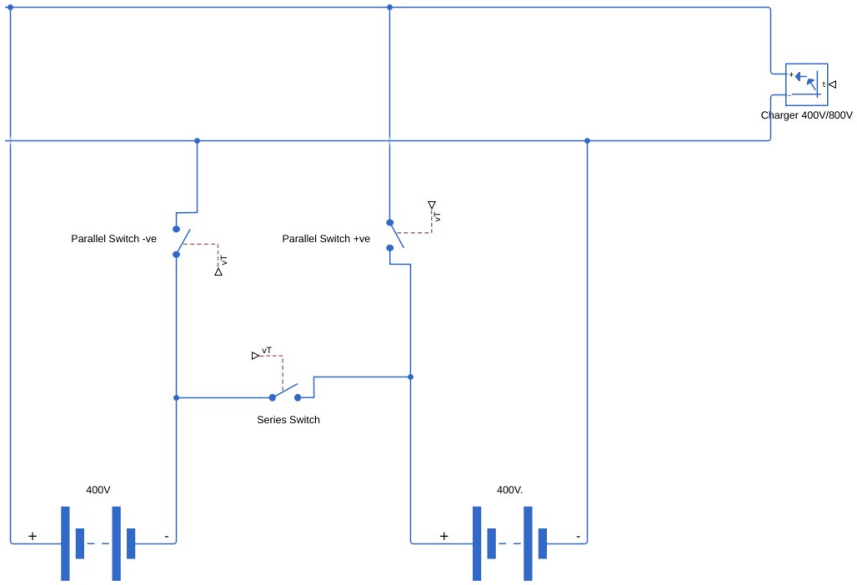

Figure 3.6: Basic principle of the Greenfield architecture

The proposed Greenfield architecture restructures the battery charging path to remove the boosting function of the inverter during low voltage DC charging. In the DC boost system, when charging from a standard 400V DC source, the EV relies on the motor inverter operating in reverse to boost voltage up to the required 800V level for battery charging. This introduces additional conversion losses, control complexity, and thermal stress into the system. The Greenfield design, on the contrary, employs a modular battery architecture in which two 400V battery modules can be connected either in series (for 800V operation) or parallel (for 400V operation). This flexibility enables direct charging from either 400V or 800V charging stations without requiring a voltage boost stage.

The Greenfield system has a BDU that replaces the booster contactor with series/-parallel switching contactors, enabling direct compatibility with 400 V charging infrastructure and eliminating the need for inverter-based voltage boosting. Table 3.1 summarises the components of both systems under review.

Table 3.1: Comparison of BDU Components in DC Boost and Greenfield Systems

Component	**DC Booster System**	**Greenfield System**	**Unit Cost(€)**	**Failure Rate PPM**	**Resistance (mΩ)**
Contactor Main +	Present	Present	15.00	0.3	0.12
Contactor Main -	Present	Present	15.00	0.3	0.12
Contactor DC Main +	Present	Present	15.00	0.3	0.12
Contactor DC Main -	Present	Present	15.00	0.3	0.12
Contactor Booster	Present	Absent	18.00	0.3	0.12
Contactor Series	Absent	Present	15.00	0.225	0.12
Contactor Parallel +	Absent	Present	15.00	0.15	0.12
Contactor Parallel -	Absent	Present	15.00	0.15	0.12
Traction Motor w/ boost	Present	Absent	800.00	–	–

In the proposed system, the batteries are arranged in parallel during 400V charging. Given that most home chargers operate at lower voltages, generally limited to 11-22kW (usually 230-400V and 16-32A) [23], the proposed system aligns with the battery configuration, enabling efficient energy transfer without requiring voltage conversion. Here, charging duration predominantly depends on charger output and SOC of the battery, with minimal internal conversion losses.

3.1.1.1 Battery Balancing

When the batteries are connected in series, the charging current passing through each module is identical. However, if one battery has a different SOC, variable degradation rate, or is simply charging faster than the other, it can become fully charged before the others. This can cause voltage imbalances, where weaker modules with lower capacity reach full charge first and risk over-voltage, potentially leading to a thermal runaway, cell degradation, or failure. Meanwhile, stronger modules with higher capacity may be underutilized, reducing the overall energy storage capacity of the battery system.

Implementing a balancing strategy ensures that the series-connected batteries reach full charge simultaneously, maximizing energy storage and preventing damage to the cells within the batteries. Design choices for balancing in high-voltage modular battery systems are guided by performance trade-offs well documented in literature. [24]. There are two methods to achieve battery balancing: passive balancing and active balancing, and the differences between them are described in Table 3.2.

Table 3.2: Passive Battery Balancing and Active Battery Balancing

Battery Balancing	
Passive Balancing	Active Balancing
Passive balancing removes extra charge from batteries that have reached maximum voltage using resistors.	Active balancing moves extra charge between battery modules using power electronics like inductors, capacitors, or transformers.
Simple, low-cost, and needs no complex circuits.	It is more efficient since energy is transferred but increases complexity in control.
Energy wasted as heat, lowering efficiency and also slow, unsuitable for fast charging.	This method balances charge faster, useful for high-power charging, and produces less heat, easing cooling demands.

3.2 Methodology

To validate the proposed system, a comprehensive methodology using simulation modelling and analytical calculations is employed.

3.2.1 Simulation model in MATLAB Simulink

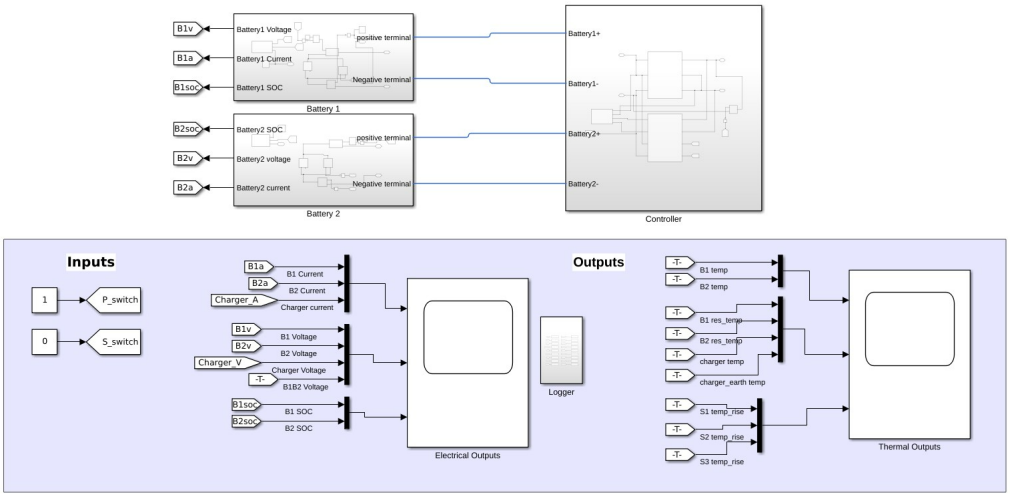

Figure 3.7: Top Level View of the MATLAB Simulink Model

The proposed model is assembled using elements from *Simscape Electrical*, with the top level illustrated in Fig. 3.7. The *Battery Equivalent Circuit* block models two battery packs, with parameters shown in table 3.3 and figure 3.8

Table 3.3: Battery Model Data and Parameters

Nominal Voltage per Module	400 V
Rated Capacity per Module	180 Ah
Initial State of Charge (SOC)	0%
Battery Heat Capacity	900 kJ/K
Impedance	28 (mΩ)

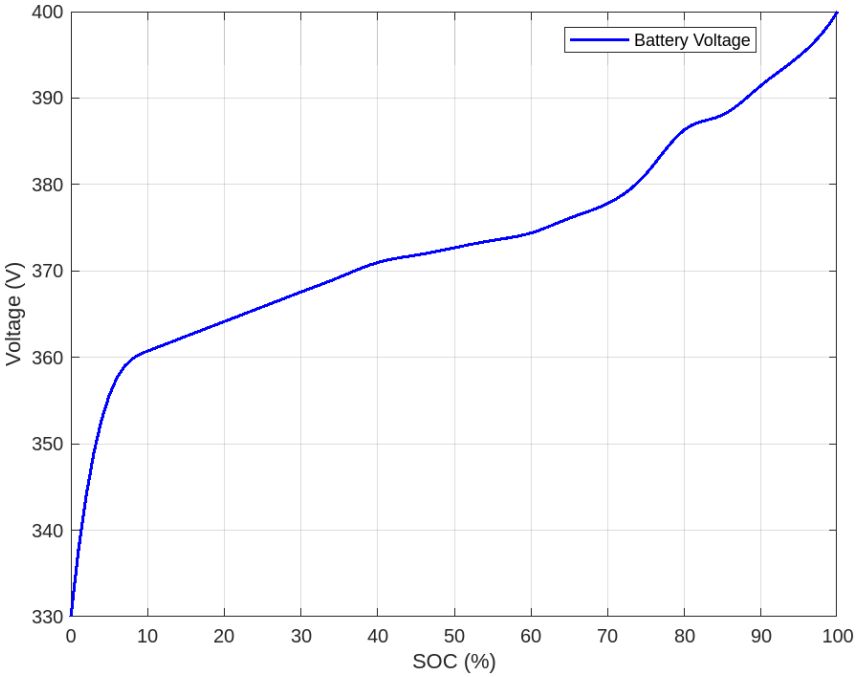

Figure 3.8: Voltage vs SOC input curve for battery modelling in the Greenfield system

Charging is modelled using a *controlled current source* block, which imposes a fixed current profile regardless of the instantaneous voltage across the terminals as shown in Fig. 3.9. The current profile is sourced from an existing charging profile. In this profile, a charging current of 250A is supplied for the initial 3126 seconds, then reduced to 60A up to 5840 seconds.

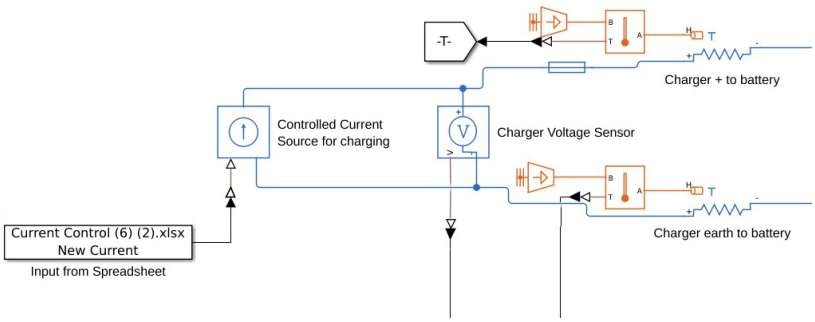

Figure 3.9: Model of the charging subsystem

The *controlled current source* used in the model gives freedom to manipulate the current supplied to the system but accompanying voltage is limited to the instantaneous voltage across the batteries at any time. Thus, scaling of the current was needed in the charging profile for the Greenfield system to match the charging power as given in (2.4) at every second for the DC boost system. This resulted in a charging current of 354A supplied to the Greenfield system for an initial 3126 seconds, then reduced to 76A up to 5840 seconds.

These parameter values are derived from actual data collected from battery packs used in production EVs. A controller subsystem is modelled to include the switching, charger, and balancer subsystems, which oversee the charging, discharging, configuration switching, and balancing of the battery packs as needed. The primary objective is to compare the 400V charging capability of the new system against the existing one. Moreover, the system is programmed to recognize the charging type based on user inputs and adjust the battery balance if the SOC difference surpasses a predetermined threshold, as depicted in Fig. 3.10.

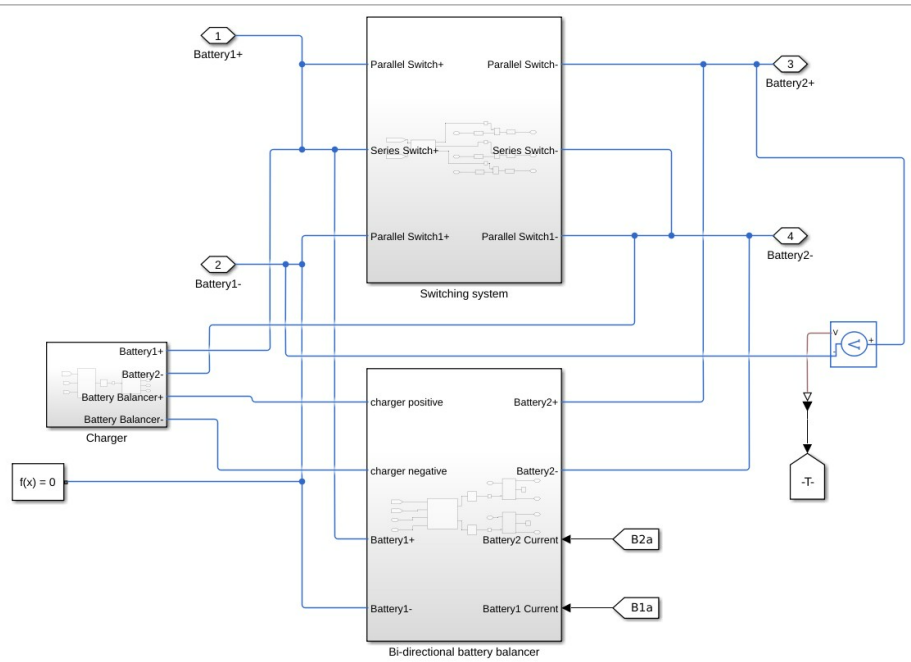

Figure 3.10: System Level View of the MATLAB Simulink Model

Since the system is modelled using a controlled current source, the input current is maintained, and the model dynamically adjusts the voltage to satisfy the power requirements. As a result, losses and variations due to system resistance and switching behaviour are reflected primarily in the voltage, which can be directly controlled within this framework. Under standard circumstances, this current is directed straight to the battery terminals. However, if the SOC disparity between battery packs surpasses a certain limit, the current is initially channelled through the battery balancing circuit prior to reaching the terminals. To achieve a more realistic simulation of actual conditions and facilitate the examination of conduction losses, the system's busbars are modelled with *thermal resistance* blocks. These resistive com-

ponents are positioned between the charger and battery terminals, among switching elements, and within alternate current pathways to address voltage drops and power losses that occur during the charging. The electrical resistance of these components was determined by measuring the resistance of the busbars in the existing BDU.

Table 3.4: Measured Busbar resistances in the BDU

Measure Points	**Resistance(mΩ)**
Cell to Main Positive Contanctor	0.194
Main Positive Contactor to Charger Connector	0.308
Cells to Main Negative Contactor	0.197
Main Negative Contactor to Charger Connector	0.023

Since the current and voltage limits for the proposed system will resemble those of the DC boost system, using the existing busbars is feasible. Therefore, similar busbar resistance is expected in the Greenfield system.

Thermal characteristics, comprising the temperature coefficient, thermal time constant, and dissipation factor, are used to simulate the thermal behaviour of the busbar.

Table 3.5: Thermal properties of BDU Busbar

Thermal Characteristic	**Value**
Reference Temperature (°C)	25
Temperature Coefficient (1/K)	0.00403
Thermal Time Constant (Seconds)	35
Dissipation factor (W/K)	15
Charger Busbar Dissipation Factor (W/K)	35

These parameters reflect the temperature increase in components and are instrumental in evaluating the system's thermal performance. They were selected according to experimental data regarding the final temperatures of the current BDU, as well as to align with the projected temperatures in the new system.

The switching system utilizes three switches, represented by the *Ideal Switch* block, to arrange the packs in either a parallel or series configuration, based on the system's requirements.

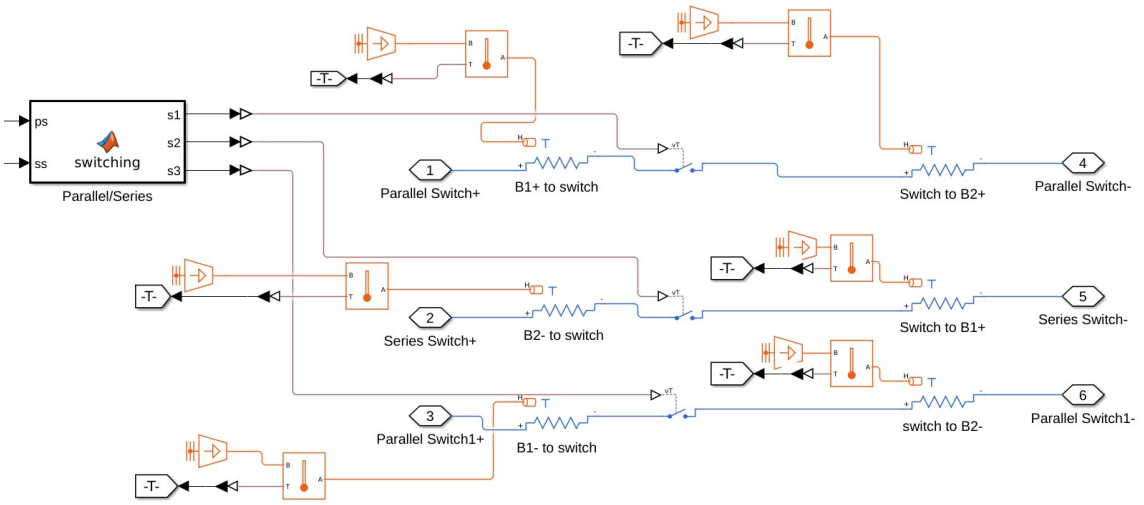

Figure 3.11: Model of Series/Parallel switching system

These switches are configured with internal resistance parameters, which are derived from the specification sheets of the contactors currently used in the BDU. Additionally, it features a function to control the enabling of switches based on user input.

3.2.2 Battery Balancing

In EVs, balancing is generally conducted at the cell level by the BMS, which continuously monitors and adjusts each individual cell state. However, this study does not include detailed cell-level modelling. Instead, the model incorporates pack-level balancing to approximate and capture essential system behaviours.

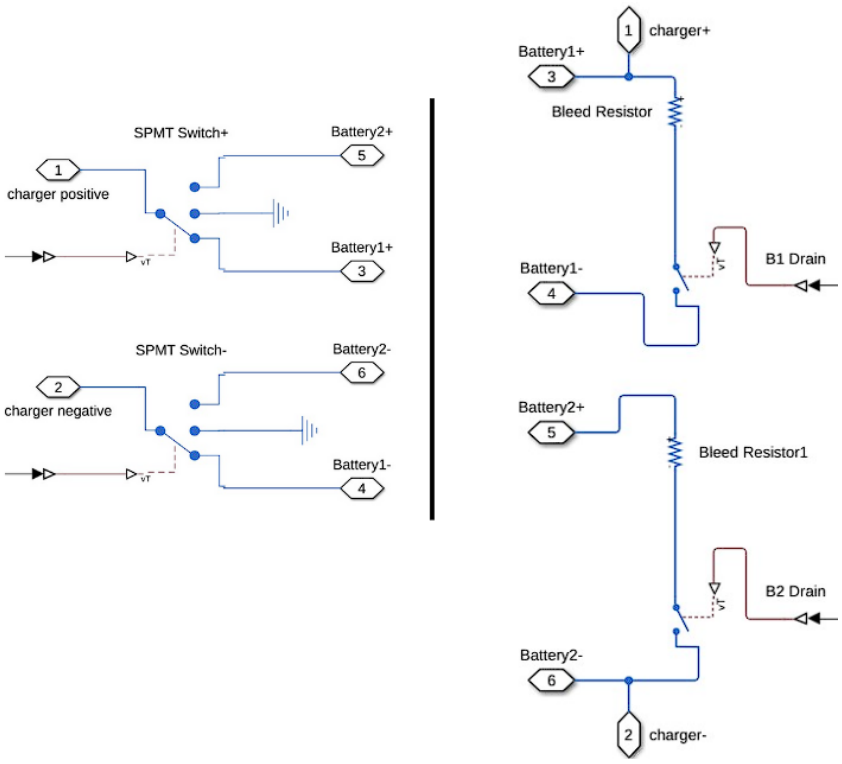

Figure 3.12: Model of active battery balancing (left) and passive battery balancing (right)

The simulation model includes both active and passive balancing strategies as shown in Fig. 3.12. Active balancing employs switches to redirect charge between packs, whereas passive balancing uses bleed resistors to dissipate energy from the higher-charged pack. These mechanisms trigger when specific SOC difference thresholds are exceeded and remain inactive during standard charge cycles when SOC is balanced.

3.2.3 Performance Evaluation

This section presents the methodology employed to assess the performance of the proposed system, providing a comparison with the existing system. The evaluation covers key metrics such as system efficiency, charging duration, thermal dynamics, reliability, and cost-effectiveness. Each of these factors significantly influences the system's long-term benefits and practical viability. By thoroughly examining these metrics using simulation results and modelled losses, a comprehensive understanding of the proposed system is achieved.

3.2.3.1 Loss Evaluation

The system's energy losses were evaluated by comparing the DC boost charging setup with the Greenfield configuration using direct 400V charging. Both systems share the same charging profile, allowing losses to be measured as the difference between input power from the charger and the energy delivered to the battery. MATLAB-based simulations incorporating electrical and thermal models were used to capture losses across battery modules, switching devices, and busbars. Using time-dependent simulations, system-level losses was calculated under 400V conditions using (2.5). This analysis highlights how design choices impact loss distribution and system performance [25].

3.2.3.2 Thermal Performance

Thermal performance is a critical factor influencing the life and reliability of power components in EV systems as high temperatures are the primary source of failure, and overheating drastically reduces reliability and lifetime [3]. While both the baseline and Greenfield system follow similar power delivery profiles, the thermal behaviour of key components differ due to changes in system architecture and current paths. The temperature rise across components over the charging cycle is analysed rather than absolute temperatures as this helps assess thermal stress and effectiveness of cooling strategies.

The thermal performance evaluation was done through simulation in MATLAB Simulink. A thermal behaviour was replicated by using *thermal resistor block* to model the busbars with the thermal parameters stated in table 3.5. The simulation environment included transient thermal analysis to capture temperature changes during 400V charging. Boundary conditions reflecting ambient temperature were applied to reflect realistic environmental effects. The thermal behaviour in the model was governed by (2.2) and (2.3) to simulate temperature distributions and temporal temperature profiles in the system. Key outputs includes maximum component temperatures and temperature gradients, which were analysed to assess the system's thermal stability and identify potential hotspots. This simulation only approach allowed a preliminary thermal evaluation, providing insight into the thermal behaviour of the proposed system and guiding future physical prototyping and thermal management design.

3.2.3.3 System Reliability

The methodology involved aggregating component-level data to assess the overall reliability impact at the system level. This included a comparative evaluation of both configurations to determine which design exhibited superior robustness in the field. The comparison focuses on the BDUs components listed in table 3.1 and their failure rates observed during the first 12 Months in Service (MIS) and projected failure rates up to the End of Life (EOL) of the vehicle.

Failure data was sourced from in-service monitoring records and validated field return reports. These records captured part-specific failure events across vehicles equipped with each system. For each component, the failure rate was expressed

in parts per million (PPM), and further normalized on a per-vehicle basis as failures per 1000 vehicles (R/1000 Vehicles). The dataset also included the quantity of each BDU component installed per vehicle, allowing for accurate aggregation and system-level analysis.

As no internal data was available regarding the long-term impact of inverter-based voltage boosting on the traction motor, a literature-based methodology was adopted to assess the reliability implications specific to the motor system using three key indicators: motor winding temperature rise, relative dV/dt stress, and partial discharge (PD) risk. These metrics quantify the electrical and thermal stress imposed on the motor during voltage boosting and are derived using the expressions previously introduced in Section 2.5.6.

This approach does not estimate failure rates numerically but allows to illustrate how voltage boosting in the DC boost system introduces elevated stress conditions that are mitigated in the Greenfield design.

3.2.3.4 Cost

In addition to evaluating the technical performance of the battery systems, it is essential to assess their economic feasibility. The analysis covers the hardware costs at the component level within the BDU and selected components associated with the transition from the DC boost system to the Greenfield system. The Greenfield system introduces new components (and eliminates a few) compared to the current architecture. Key hardware differences are summarized in table.

Table 3.6: Hardware Cost Breakdown

Component	**DC boost System**	**Greenfield System**
Battery Pack	Single 800V Pack	Two 400V Modules
Motor	Rear motor with voltage boost function	Voltage boost function is removed
Contactors	Main, DC & Booster contactors	Main, DC & Series/Parallel contactors

All other BDU components not explicitly discussed, such as fuses, housing, high-voltage connectors, and standard monitoring circuitry, are assumed to remain unchanged between the current and Greenfield systems. Their cost impact is therefore considered neutral in this comparison.

3.2.3.5 Sensitivity analysis

To evaluate the robustness and behaviour of the proposed battery system under varying conditions, a sensitivity analysis was conducted. Three specific scenarios was conducted as shown in table . These cases were selected to analyse the impact on the chosen performance metrics, helping to identify design trade-offs and validate the flexibility of the proposed architecture under practical constraints.

Table 3.7: Sensitivity analysis scenarios

Sensitivity Scenario	**Description**
Constant current source	250A fed into the system throughout the runtime
SOC imbalance	Initial SOCs of the two battery modules are unequal. Batteries configured in series to trigger balancing
Replacing Aluminium with Copper	Resistance value in the model factorized to match the material change

4
Analysis

4.1 System Performance Evaluation

This chapter offers a comparative evaluation of 400V charging in the current and Greenfield systems. The comparison excludes 800V DC fast charging since both systems utilize the same charging design.

Key performance indicators such as voltage, current and efficiency were analysed. Subsequent sections further explore the effects of stress on component longevity, detailing how the Greenfield system enhances the durability of components. This section also offers insights into the cost disparities between the systems.

4.2 Simulation Results Insights

4.2.1 Electrical Performance

Fig. 4.1a depicts how battery charging current correlates with state of charge (SOC) during a varying current profile. The graph initially demonstrates a gradual reduction in charging current from about 178A to 158A as the SOC progresses from 0 to approximately 80%, signifying a controlled tapering phase that corresponds with typical constant current–constant voltage (CC–CV) charging protocols. Once SOC reaches 80%, the current sharply reduces to 40A, signaling the beginning of the constant voltage phase, where current is significantly curtailed to prevent overcharging and thermal stress. This approach promotes battery life by minimizing electrochemical stress in the high SOC regions [31]. Analysing this curve allows for an assessment of the charger's regulation approach, the impact on thermal management, and its efficiency under varying load conditions. Moreover, it assists in pinpointing current tapering inflection points that could be optimized for quicker yet safe charging, particularly if thermal limits or reliability boundaries are nearing design constraints.

In the proposed system, the charger current is dynamically divided across the two battery packs based on configuration mode. During 400V charging, the system operates in parallel, with each battery receiving half the total charger current, shown in Fig. 4.1b, where current at each battery terminal mirrors this division during both constant current and tapering phases. This setup reduces current stress per pack, lowering resistive losses and heat generation as per (2.1), which improves thermal performance and supports longer component life [26, 27, 20]. Additionally, parallel operation avoids charge imbalance [28]. However, implementing this flexibility

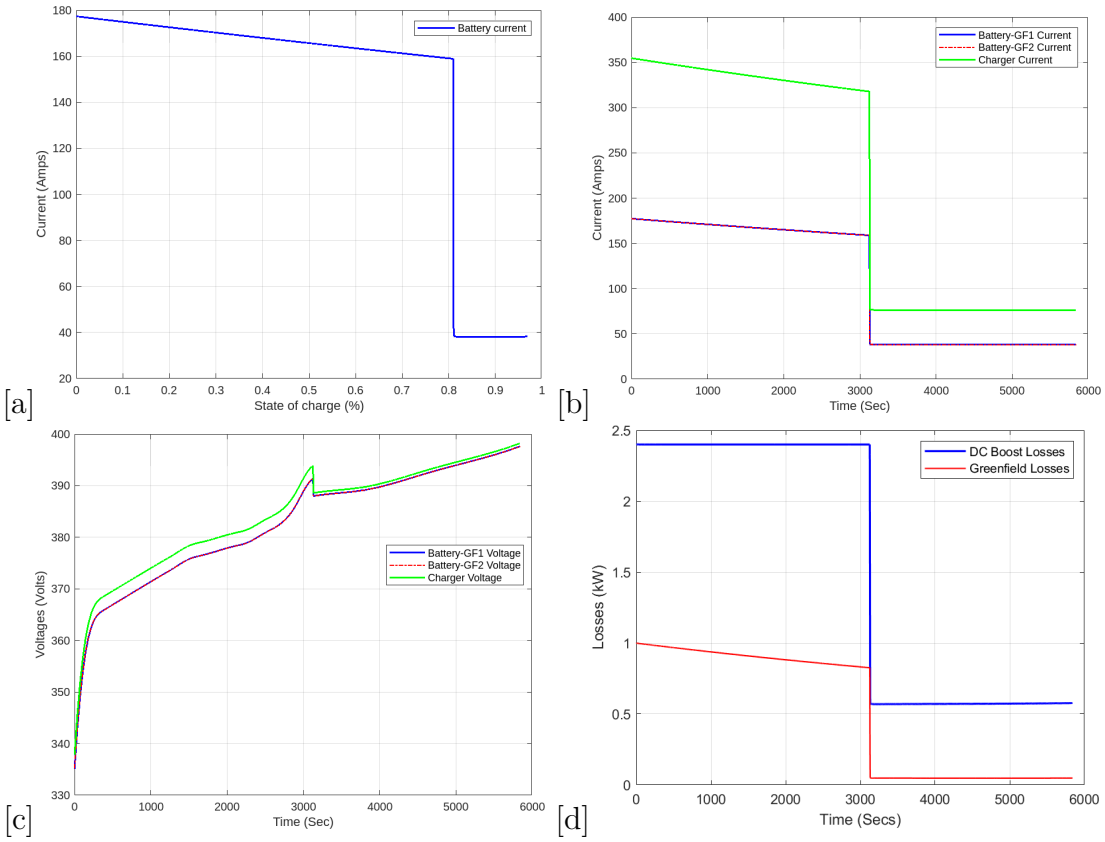

Figure 4.1: (a) SOC vs current (b) Charging profile and battery currents (c) Battery voltage vs time (d) System losses comparison

requires additional switching mechanisms and precise SOC management to prevent imbalance when transitioning to series mode for 800V operation [37]. Despite these trade-offs, the proposed configuration supports modular, voltage-adaptive charging and demonstrates accurate current distribution—an essential feature for system reliability and next-generation EV architecture [3].

The voltage dynamics between the charger and battery terminals in the proposed system were evaluated to determine resistive losses. Utilizing a *controlled current source* in the model causes losses to manifest as a difference in voltage between that of the charger and the batteries as shown in Fig. 4.1c. At lower currents (due to tapering), these differences decrease, indicating more efficient energy transfer. As the voltage nears full SOC, the slope of the curve levels out, indicating reduced power input and increased battery impedance at near full SOC [35]. This gradual flattening of the curve underscores the effects of rising internal resistance and the significance of tapering the current to achieve voltage regulation.

Comparing the system losses of the DC boost and Greenfield systems reveals stark differences in overall losses as calculated by (2.5), with temporal results for the Greenfield system and DC boost system shown in Fig. 4.1d. The Greenfield system follows an overall trend of lower losses throughout the entire simulation period, consistent with (2.1), as conduction losses in busbars, connectors, and internal resistances dominate energy loss [3]. The DC boost system has a loss of around 2.5KW at higher currents while tapering down to 0.6kW at lower currents, while the Greenfield system, despite operating at lower voltage and higher current, shows a reduced loss of 1kW to just 0.1kW as current decreases. This behaviour is primarily due to the absence of a boost converter stage in the Greenfield system, eliminating switching losses and leaving only current-dependent conduction losses. In contrast, the DC boost system incurs higher losses from voltage conversion, leading to an elevated loss profile. Despite architectural differences, both systems deliver roughly the same power. These results confirm that, while the Greenfield system introduces a different approach, it effectively lowers system losses, thereby validating its viability as a modular alternative for future electric vehicle (EV) platforms.

Considering the time step 1124 sec, The current across the batteries were 170.25A and the voltages across the batteries were 372.45V. On the charger side, the voltage was 375V and current was 340.5A. Using (2.4) and (2.5), we calculate the losses at this particular timestep.

On the battery side, the output power would be the sum of individual powers of the battery.

$$P_{out} = V_{GF1} \times I_{GF2} + V_{GF2} \times I_{GF2} = 2 \times (372.45 \times 170.25) = 126.82kW \tag{4.1}$$

$$P_{in} = V_{charger} \times I_{charger} = 375 \times 340.5 = 127.71kW \tag{4.2}$$

$$Losses = P_{in} - P_{out} = 127.71 - 126.82 = 0.89kW \tag{4.3}$$

4.2.2 Thermal Performance

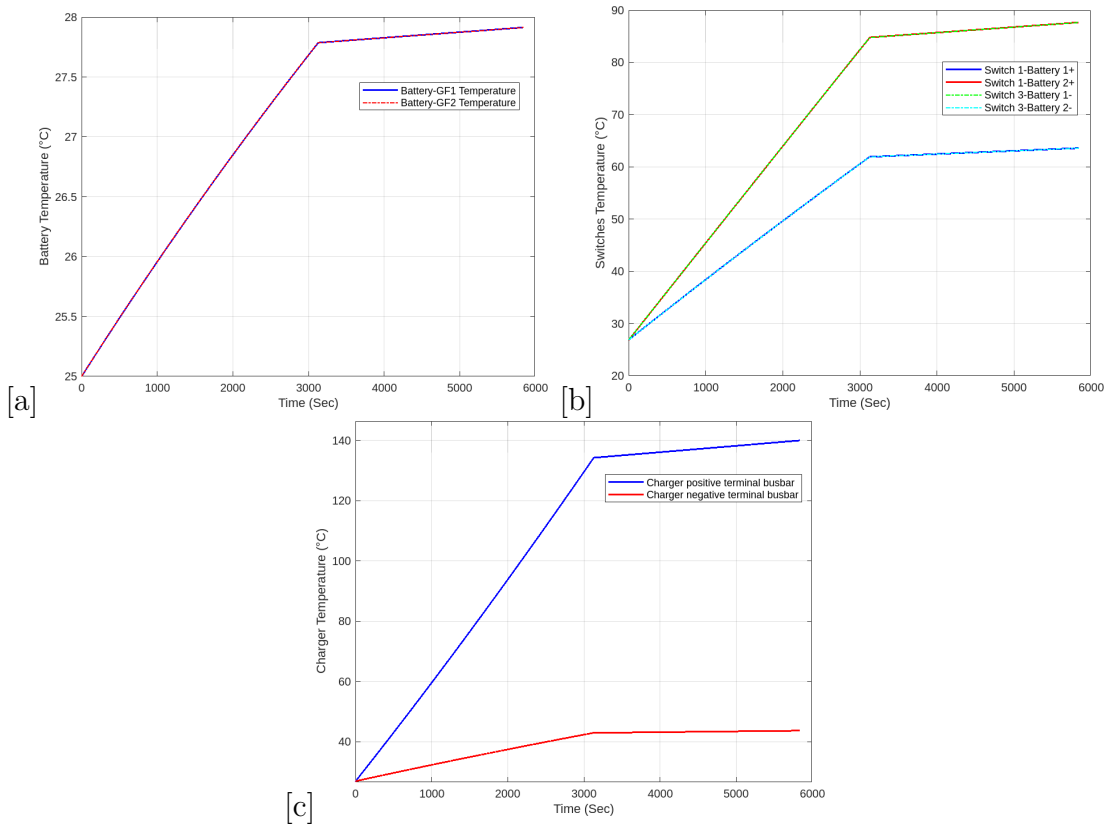

Figure 4.2: (a) Battery temperatures vs time (b) Switch busbar temperatures vs time (c) Charger busbar temperatures vs time

Thermal analysis on the proposed system highlights notable differences in the thermal behaviour, particularly around the busbars of the charger terminals. For this analysis, the ambient temperature was assumed to be 25°C. The battery packs show a moderate and uniform temperature rise from 25°C to 31°C as shown in Fig. 4.2a, indicating that despite differences in charging methodology, the core battery thermal response remains within safe limits due to their relatively large thermal mass and thermal management systems [33].

For the total simulation period of 5840 seconds, the resistance of the busbars change according to the temperature of the busbar governed by (2.2). After the temperature-dependent resistance is calculated, (2.3) is used to calculate the temporal heat rise in the busbar.
For example, consider the switching system "switch 3" busbar given in Fig. 4.2b with $R_0 = 0.194$ mΩ, $T_0 = 25°\text{C}$, $\alpha = 0.00403$ K^{-1}, $I_b = 160$ A, $K_d = 15$ W/K, and $t_c = 35$ s. At $T = 88°\text{C}$, the resistance increases to:

$$R(88) = 0.000194 \cdot (1 + 0.00403 \cdot (88 - 25)) = 0.000243\ \Omega$$

The power loss using 2.1 becomes $P = I^2R = 160^2 \cdot 0.000243 = 6.22$ W. Using 2.3, the rate of temperature rise is:

$$\frac{dT}{dt} = \frac{6.22}{K_d \cdot tc} = \frac{6.22}{525} \approx 0.011 \text{ K/s}$$

This demonstrates that the temperature increases gradually due to thermal inertia. As the temperature increases further, resistance and losses rise until the heat dissipated equals the heat generated, resulting in a steady-state condition. This accurately captures dynamic thermal effects and validates the design's response under high current loading.

The busbars connecting the battery packs to the switches reveal asymmetrical temperature profiles. Specifically, the positive terminal of Battery 2 and the negative terminal of Battery 1 both exhibit a steep rise from 25°C to 88°C, whereas their respective counterparts rise only to 64°C as shown in Fig. 4.2b. This difference could be attributed to the assumed asymmetrical physical placement of busbars in the BDU. Longer or more complex routing of certain busbars, due to mechanical layout constraints, results in higher losses and reduced convective cooling, thereby elevating local temperatures [34]. Although all busbars were assigned the same thermal time constant for modelling simplicity, design-induced differences in heat dissipation and resistance values can lead to significant variations in thermal build-up.

The most critical observation occurs at the charger side. The positive charger busbar sees the highest temperature rise, from 25°C to 140°C, approaching the established thermal limit of 150°C. In contrast, the negative side experiences a more modest rise, reaching only 44°C as shown in Fig. 4.2c. This asymmetry likely arises from higher current densities and different resistance values of the busbars stemming from the design and packaging of the BDU. This underscores a potential reliability concern under sustained high current charging conditions [33].

4.2.3 Reliability

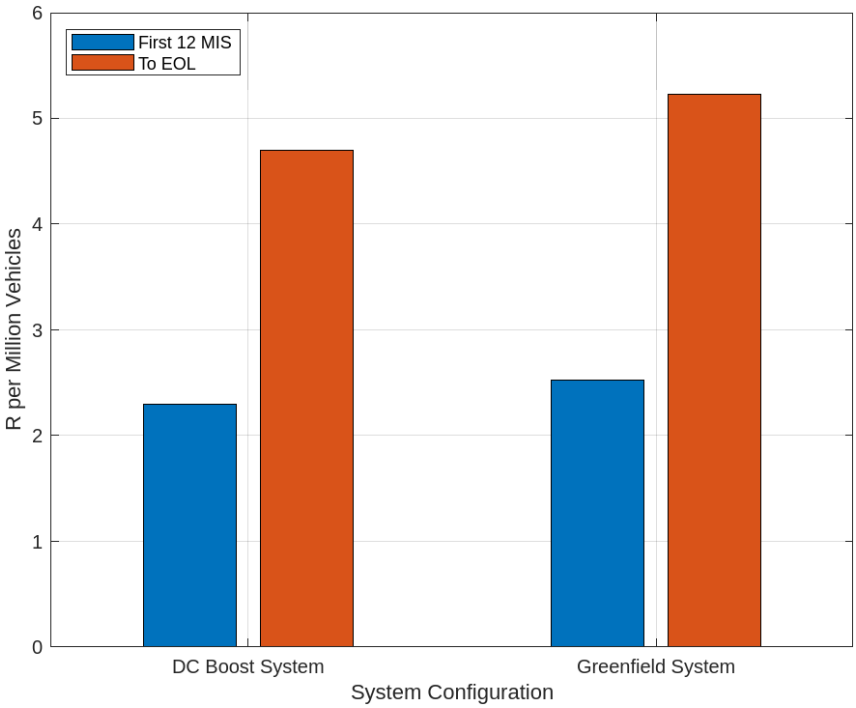

Figure 4.3: Reliability Comparison: DC Boost vs Greenfield System

To evaluate the reliability impact of the two system architectures, failure rates of individual BDU components were aggregated to a system-level reliability index. The approach leverages field failure data, expressed in parts per million (PPM), as listed in Table 3.1. These figures represent observed or projected failures over the vehicle lifetime, either within the first 12 months in service (MIS) or up to end-of-life (EOL), normalized across the vehicle population.

Each contactor's failure rate (in PPM) was multiplied by the number of units per vehicle for that configuration, and the results were summed to obtain an overall reliability figure per million vehicles. The failure contributions were calculated separately for the DC boost and greenfield systems.

The DC booster system includes the following components:

- 2 Main contactors: $2 \times 0.3 = 0.6$ PPM
- 2 DC Main contactors: $2 \times 0.3 = 0.6$ PPM
- 1 Booster contactor: $1 \times 0.3 = 0.3$ PPM

$$\text{Total System Failure Rate}_{\text{DCBoost}} = 0.6 + 0.6 + 0.3 = \boxed{1.5 \text{ PPM}}$$

When projected across 1 million vehicles, this gives:

$$R_{\text{DCBoost}} = 1.5 \times 10^6 \text{ failures/million vehicles}$$

For visualization purposes, Fig. 4.3 further extrapolates this to the full EOL profile, the failure rates for other components such as the fuses and pyrofuse were added to the aggregation.

The greenfield configuration eliminates the booster contactor but introduces three additional units for switching:

- 2 Main contactors: $2 \times 0.3 = 0.6$ PPM
- 2 DC Main contactors: $2 \times 0.3 = 0.6$ PPM
- 1 Series contactor: $1 \times 0.225 = 0.225$ PPM
- 2 Parallel contactors: $2 \times 0.15 = 0.3$ PPM

$$\text{Total System Failure Rate}_{\text{Greenfield}} = 0.6 + 0.6 + 0.225 + 0.3 = \boxed{1.725 \text{ PPM}}$$

This yields a slightly higher base-level failure rate compared to the DC Boost system.

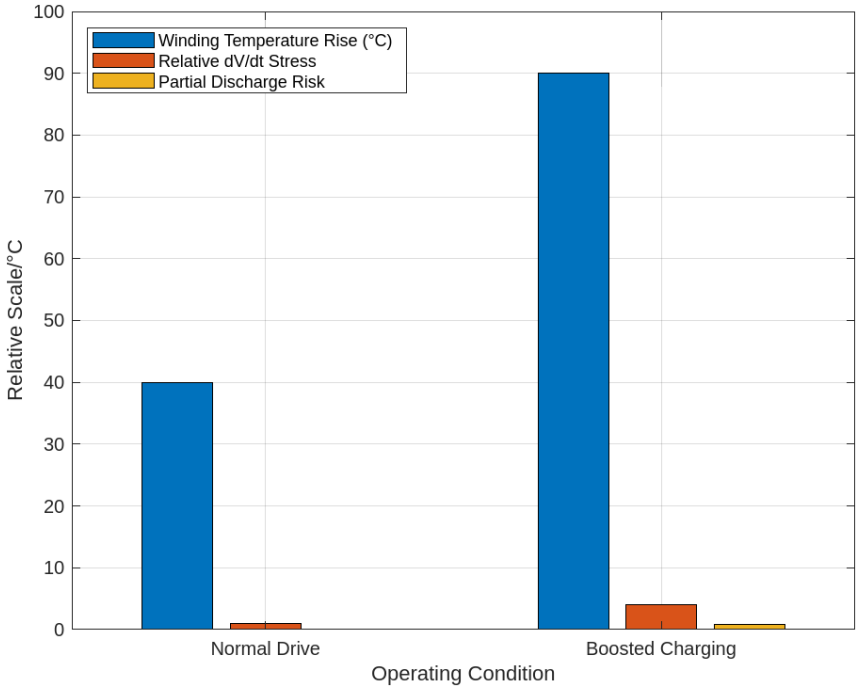

Figure 4.4: Effect of Voltage Boosting on Motor Stress Indicators

The stress indicator values presented in the in Fig. 4.4, winding temperature rise, relative dV/dt stress, and partial discharge (PD) risk are derived using the theoretical expressions introduced in Section 2.5.5. These indicators were calculated using literature-based system parameters, scaled with appropriate calibration factors, to reflect practical motor operating conditions.
The winding temperature rise is calculated using the empirical loss-based expression in (2.6). This formulation is based on simplified thermal modeling of ohmic and magnetic losses in the stator, following the approach of Ji et al.[22]. The calibration factor k accounts for heat rejection dynamics in the motor housing and coolant path.

Normal Drive

- $I = 150\,\text{A}$, $R = 0.01\,\Omega$, $\eta_{\text{loss}} = 0.85$
- $f_{\text{sw}} = 5\,\text{kHz}$, $C_{\text{core}} = 0.002\,^{\circ}\text{C/kHz}$
- Raw: $\Delta T_{\text{raw}} = 191.26$

- Calibrated with $k = 0.209$:

$$\Delta T_{\text{actual}} = 0.209 \cdot 191.26 \approx \boxed{40\,^\circ\text{C}}$$

Boosted Charging

- $I = 250\,\text{A}$, $f_{\text{sw}} = 20\,\text{kHz}$
- Raw: $\Delta T_{\text{raw}} = 531.29$
- Calibrated with $k = 0.169$:

$$\Delta T_{\text{actual}} = 0.169 \cdot 531.29 \approx \boxed{90\,^\circ\text{C}}$$

Relative switching stress is defined as the ratio of peak dV/dt levels during voltage boosting and normal drive as expressed in (2.7). In typical EV operation, the inverter switching rate under normal drive is approximately $2.5\,\text{kV}/\mu\text{s}$, while under boosting it can reach up to $10\,\text{kV}/\mu\text{s}$ in systems using wide-bandgap devices such as SiC MOSFETs [22].

$$\text{Relative Stress} = \frac{10}{2.5} = \boxed{4.0}$$

The partial discharge (PD) risk is estimated using the proportional relation presented in (2.8)

Experimental data in Ji et al.[22] shows that PDIV decreases significantly as insulation is thermally aged and repeatedly exposed to high-frequency switching. Using $\text{PDIV}_{\text{initial}} = 12\,\text{kV}$, the risk index is calculated for both cases:

Normal Drive:

$$\frac{40 \cdot 2.5}{12} = 8.33 \quad \Rightarrow \quad \text{Normalized Risk} \approx \boxed{0.1}$$

Boosted Charging:

$$\frac{90 \cdot 10}{12} = 75.0 \quad \Rightarrow \quad \text{Normalized Risk} \approx \boxed{0.8}$$

This sharp increase reflects the elevated exposure of stator insulation to thermal and electrical stress under voltage boosting conditions. By removing boosting in the greenfield system, this degradation pathway is effectively eliminated.

4.2.4 Cost Analysis

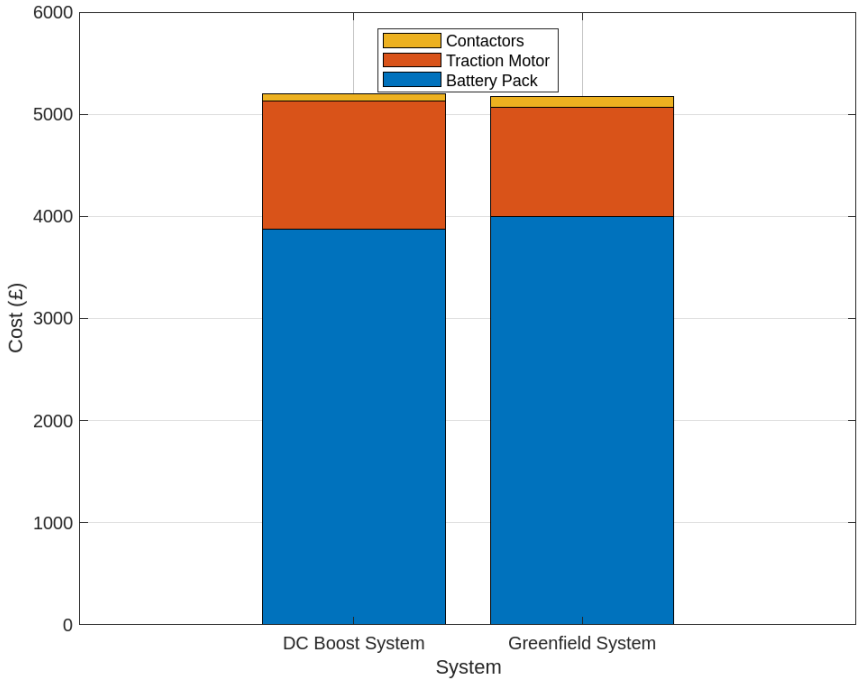

Figure 4.5: Component Cost Comparison Between DC Boost and Greenfield Systems

Component-level cost estimates were based on supplier catalogues and proportional scaling from known reference prices. Each cost value reflects the per-unit cost of the component, multiplied by the quantity used per vehicle. The results are summarized visually in Fig. 4.5, which highlights the distribution of total cost across the three main subsystems.

Table 4.1: Hardware Cost Comparison Between Current and Proposed Systems

Component	DC boost System	Greenfield System	Cost Impact
Battery Pack	Single 800V Pack	Two 400V Modules	Small cost increase
Motor	Rear motor with voltage boost function	Voltage boost function is removed	Cost Savings
Contactors	Main, DC & Booster contactors	Main, DC & Series/-Parallel contactors	Cost increase

Both systems use two physical battery packs in series. However, the greenfield system introduces modular switching logic to allow dynamic reconfiguration between series and parallel. This adds minor cost for interconnects and control, resulting in a small increase from approximately €3900 to €4000 per vehicle.

The motor in the DC Boost system is oversized for voltage boosting capability, requiring additional insulation and inverter integration. In the greenfield design,

this functionality is removed, simplifying the motor and reducing cost, this change yields a savings of approximately €200.

The DC Boost system uses five contactors (main, DC, and booster), while the greenfield system replaces the booster contactor with three new switching contactors (series, parallel+, and parallel–). Although the booster contactor is slightly more expensive than a standard unit, the added contactors in the greenfield system result in a net increase in contactor-related cost from €75 to approximately €105.

The net result is that both systems incur similar total hardware costs, with a marginal increase in contactor and battery costs in the Greenfield system. However, the cost increase is offset by simplification in the motor subsystem and the elimination of the inverter-assisted charging pathway, which may reduce long-term integration and service costs.

4.3 Sensitivity Analysis

To further evaluate the robustness and adaptability of the proposed system, a sensitivity analysis is conducted by altering key system parameters and operating conditions mentioned in Table 3.7. This analysis explores how different configurations influence system performance across five critical metrics: current behaviour, voltage response, SOC evolution, charging efficiency, and thermal performance.

The first scenario tests the system's behaviour under a steady load, helping isolate effects that tapering naturally compensates for, such as thermal relief and energy optimization. The goal of the second scenario was to examine how both active and passive balancing strategies manage SOC discrepancies during a full charging cycle. The third scenario helps quantify the trade-offs between thermal rise, and electrical efficiency, providing insight into whether such a substitution could enhance reliability and thermal performance.

4.3.1 Constant Current Source

To analyse the sensitivity of the model towards current input changes, the existing *controlled current source* block was replaced with *current source* block with a constant DC current of 250A, the performance of the model was analysed and the following performance indicators were analysed.

4.3.1.1 Efficiency

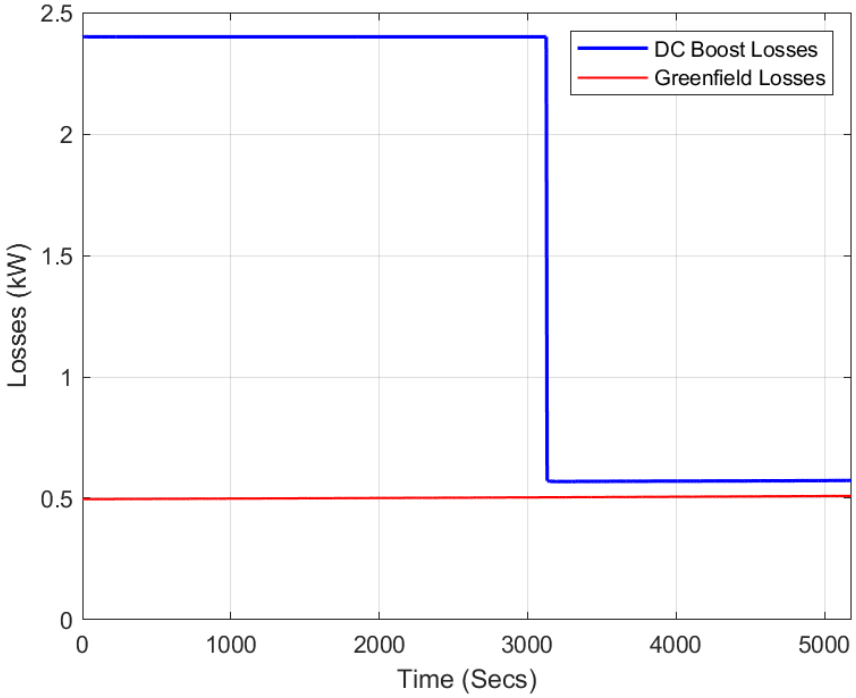

Figure 4.6: System Losses vs time

The efficiency under constant current shows a slight decline compared to the dynamic profile as shown in Fig. 4.6, and is seen to mimic the voltage curve. This is due to uninterrupted high conduction losses, as resistive elements dissipate more power under sustained load. Unlike real conditions where current drops periodically for electrical and thermal recovery, this setup maintains peak stress continuously, causing a lower average efficiency. The differences remain marginal due to the same end-to-end power delivery and minimal architectural changes in the BDU [38].

4.3.2 Unbalanced Battery Conditions

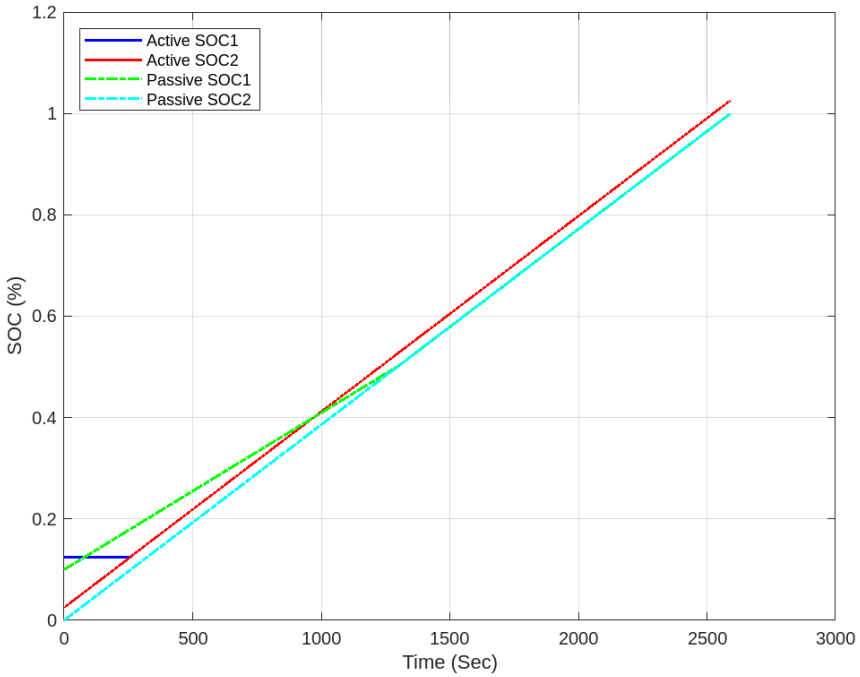

Figure 4.7: Active vs Passive Battery Balancing

The resulting SOC convergence for both batteries under each strategy is illustrated in Fig. 4.7. As shown, the active balancing method equalizes the SOCs quicker compared to the passive balancing which achieves SOC convergence in more than six times that of the active balancing method.

4.3.3 Substitution of Aluminium with Copper Busbars

The choice of busbar material has a significant impact on the system's electrical efficiency and thermal performance. Aluminium is often used due to its lower cost and weight, however, copper offers superior electrical and thermal conductivity.

This section investigates the effect of replacing aluminium busbars with copper ones, keeping all other thermal and system parameters constant. The aim is to assess how this material change influences key performance characteristics during a charging event. The resistance was decreased by a factor of 0.62 [41] to change the busbar material to copper while keeping other parameters unchanged.

By comparing simulation results from both scenarios, the aim was to determine whether the improved conductivity of copper translates into measurable benefits for the charging system and if the performance gains justify the potential trade-off in cost and weight.

4.3.3.1 Thermal Performance

This is where the most noticeable improvement is observed. Copper's higher thermal conductivity enables faster heat dissipation, leading to significantly lower peak

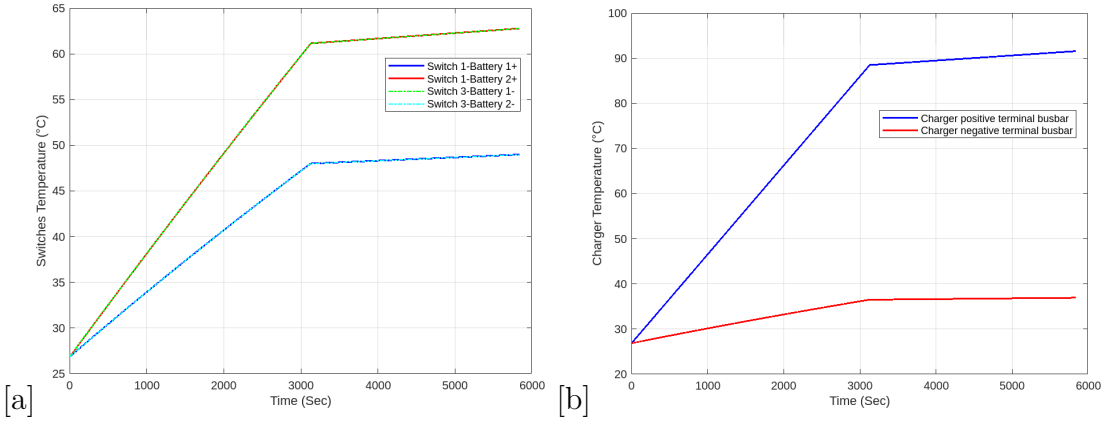

Figure 4.8: (a) Switch busbar temperatures vs time (b) Charger busbar temperatures vs time

temperatures across all busbars. The graphs as shown in Fig. 4.8, shows a consistent drop in peak temperatures compared to the baseline configuration, with reductions ranging from 15°C to 20°C across the critical busbars at switch terminals and charger interface.

Although, the thermal parameters such as dissipation factor and time constant were kept constant in the simulation model, the reduced electrical conduction losses in the copper busbars lead to lower thermal loads. This highlights copper's advantage in thermally constrained environments where sustained high current operation risks approaching material thermal limits [45]. The temperature reduction also improves system safety margins and long term reliability, particularly at charger terminals where the baseline configuration approached critical limits.

4.4 Improvements Proposal

This dual-module strategy is in line with recent industry developments: for example, the GMC Hummer EV uses two 400 V battery layers that switch to an 800 V series configuration during DC fast charging. Eaton introduced a Battery Configuration Switch (BCS) device that enables exactly this kind of series/parallel pack reconfiguration for EVs. In drive mode, the device connects two 400 V sub-packs in series for an 800 V output, and when a lower voltage is needed it switches to two sub-packs in parallel (each 400 V), allowing charging on 400 V stations [46].

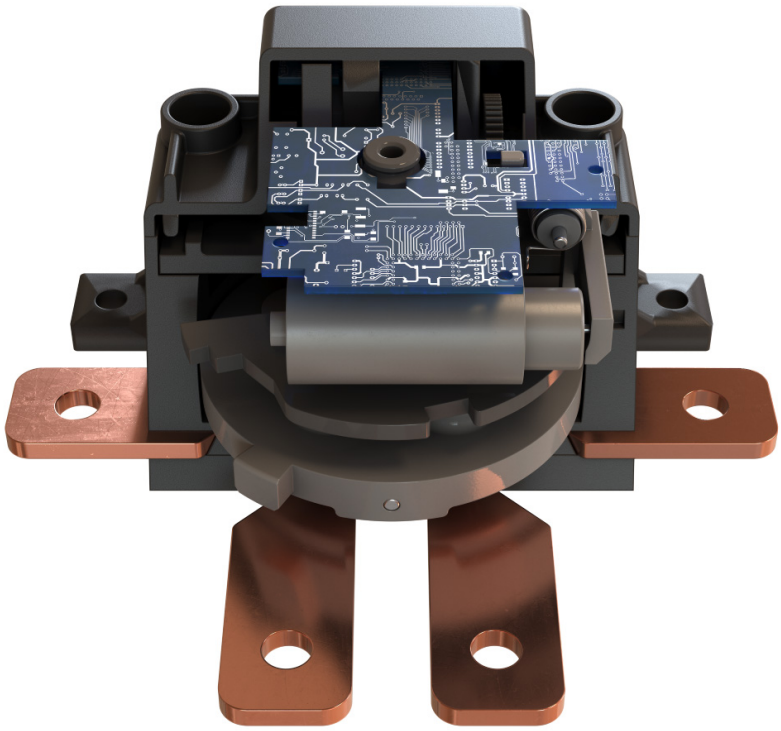

Figure 4.9: Battery Configuration Switch by Eaton

The presence of such commercial solutions lends credibility to the feasibility of the proposed architecture. Furthermore, the ability to charge on both existing 400 V infrastructure and newer 800 V chargers gives the vehicle maximum flexibility. As of 2024, only about 5% of about 2,000,000 public DC fast chargers worldwide supported 800 V charging [47].

Any significant architectural change brings associated trade-offs, one consideration is the added complexity in control logic and safety. Managing a reconfigurable battery requires a sophisticated BMS strategy. The BMS must decide when and how to transition between series and parallel configurations, and it must do so safely. Before connecting the two sub-modules in parallel, their voltages (and SOCs) need to be nearly equal; otherwise, a large circulating current could flow as they balance each other. This not only stresses the cells and inter-connectors but also wastes energy as heat during the rapid redistribution of charge. To mitigate this, the BMS should allow the contactors to close for parallel configuration if the voltage difference is below a safe threshold.

Another trade-off is the increased part count and complexity of hardware. The single-voltage pack typically uses two or three high-voltage contactors (positive, negative, voltage boost and sometimes a pre-charge contactor). In the dual-module design, it requires additional contactors to orchestrate series/parallel switching. In the proposed implementation, there is a higher component count, which impacts both cost and reliability (each contactor is a potential failure point). A mitigation

to this could be using bi-stable contactors – devices that latch in position without continuous coil power – to reduce the chances of failure and eliminate coil energy draw. The earlier reference to Eaton's BCS is relevant here: that device consolidates the functionality of multiple contactors into a single integrated unit as illustrated in Fig. 4.10.

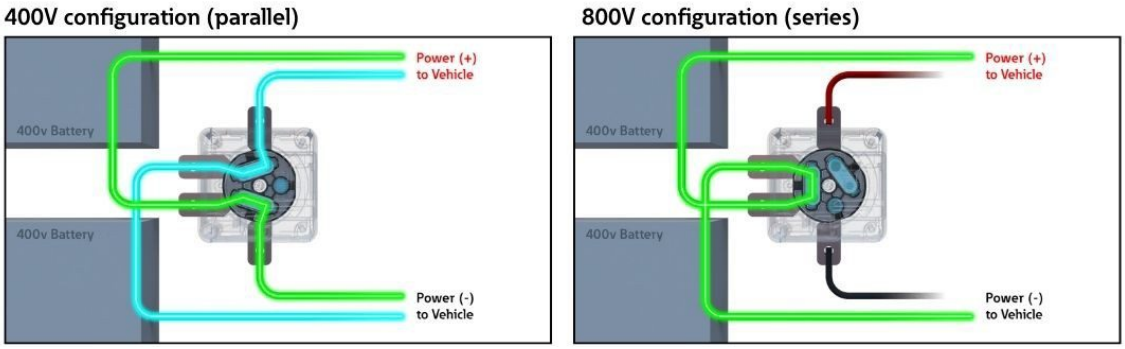

Figure 4.10: BCS Architecture by Eaton

The increase in component count is a clear trade-off: more components mean more things to design, package, and potentially service. From a cost perspective, the added contactors do incur an extra expense, partly offset by the removal of the inverter-based charger components and the DC/DC converter. The overall complexity in terms of wiring and harnesses is assumed to rise modestly. For instance, additional sense wires and drivers are needed for the extra contactors, and the pack needs a more complex high-voltage interconnect layout. These drawbacks are the price for the enhanced functionality. The design philosophy here is that the modular pack approach shifts complexity from power electronics to mechanical/electrical reconfiguration, which is justified only if the net system benefits (efficiency, reliability, compatibility) outweigh the added hardware. Analysis supports this to be the case, but the trade-off must be acknowledged.

The effective thermal and electrical performance of busbars is vital in high-power energy systems, particularly in electric vehicles. While aluminium is frequently used because of its lightweight nature and economic benefits, it offers less electrical and thermal conductivity than copper, potentially leading to greater resistive losses and heat generation. Utilising copper where it is viable to exploit its excellent thermal conductivity, keeping in mind the trade-offs in cost and weight. Moreover, improvements can be further achieved by levelling out current paths through optimised switch placement or topology changes, thus balancing thermal loads and reducing localised hotspots that threaten component longevity and system safety.

5
Conclusion

5.1 Summary

This thesis conducted a comparative evaluation of two electric vehicle battery system architecture under 400V charging, The DC boost system which uses a inverter based voltage boosting and the proposed Greenfield system employing switchable series-parallel configuration. Simulation results show that both systems accumulate different power losses, a peak of 2.5kW for the DC boost system and up to 1kW for the proposed system during higher current phase, implying that Greenfield system significantly reduces thermal stress. The most critical thermal point, the charger positive side busbar, peaked at 140°C in the Greenfield model, still within safe operational limits but highlighting the need for improved thermal management. In terms of charging effectiveness, the inverter based system achieved a nearly full SOC over the simulation period, whereas the Greenfield system reached close but could not equal the DC boost system, this is due to higher conduction losses at increased currents required for the same power transfer.

Reliability analysis also indicated a reduction in motor stress and partial discharge risks by removing the voltage boost path in the Greenfield system, although the additional contactors slightly increased component count and failure probability (0.0052 R/1000 vs 0.0047 R/1000). The analysis demonstrated that inverter-based voltage boosting significantly increases thermal and electrical stress on the traction motor. Under boosted charging conditions, winding temperature rise was estimated at approximately 90°C, more than double the 40°C observed during normal drive. Similarly, the relative dV/dt stress increased by a factor of 4, and the partial discharge (PD) risk index rose from 0.1 to 0.8, based on insulation aging models and switching transients. These indicators point to a higher likelihood of premature insulation degradation and reduced motor lifespan in the DC Boost system.

The component-level cost comparison revealed that the greenfield system incurs only a marginal increase in total hardware cost—rising from approximately €5,200 in the current system to €5,240. This increase is primarily due to the addition of series-parallel contactors (€15 each) in the BDU, which replace the more expensive booster contactor (€18) but expand the total contactor count. On the other hand, the removal of the voltage boost function in the traction motor reduces its cost by an estimated €200, partially offsetting the increase. Battery pack costs remained nearly identical between configurations. Overall, the greenfield system introduces slight added complexity in switching logic, but it balances this with architectural simplification, long-term maintainability, and improved thermal and reliability per-

formance.

5.2 Future Work

Some of the future work that could further this study would be modelling the battery pack at a cell level and implementing a cell level balancing with thermal-electrical coupling which could reveal localized imbalances and thermal runaway risks, potentially reducing balancing time by up to 30-40% compared to pack level control. Incorporating ageing models for contactors and busbars based on thermal cycling data could allow for estimation of component life under repeating switching, such as predicting contactor failure after 500,000 cycles at peak temperature loads.

A valuable extension would be to develop and simulate fault tolerant switching strategies that can bypass a failed module or switch while maintaining system functionality, improving system availability under degraded conditions. Additionally, exploring MOSFET based solid state switching as a replacement for electrochemical contactors could cut switching losses and response time, provided future solid state switches achieve full galvanic isolation.

Finally, hardware-in-the-loop (HIL) validation of the model using real battery modules and switching components would bridge the gap between simulation and implementation, and enable dynamic efficiency, temperature, and reliability measurement under real load conditions.

Bibliography

[1] Aghabali, I., Bauman, J., Kollmeyer, P. J., Wang, Y., Bilgin, B., & Emadi, A. (2021). 800-V electric vehicle powertrains: Review and analysis of benefits, challenges, and future trends. IEEE Transactions on Transportation Electrification, 7(3), 927–940.

[2] Z.-k. Chen and G. J. Witter, "Electrical Contacts for Automotive Applications: A Review," IEEE Transactions on Components, Packaging and Manufacturing Technology, vol. 11, no. 6, pp. 923–935, Jun. 2021. DOI: 10.1109/TCPMT.2021.3075635.

[3] J. Reimers, L. Dorn-Gomba, C. Mak and A. Emadi, "Automotive Traction Inverters: Current Status and Future Trends," in IEEE Transactions on Vehicular Technology, vol. 68, no. 4, pp. 3337-3350, April 2019, doi: 10.1109/TVT.2019.2897899.

[4] Han, Weiji & Wik, Torsten & Kersten, Anton & Dong, Guangzhong & Zou, Changfu. (2020). Next-Generation Battery Management Systems: Dynamic Reconfiguration. IEEE Industrial Electronics Magazine. 14. 10.1109/MIE.2020.3002486.

[5] Blaabjerg, F. & Wang, Huai & Vernica, Ionut & Liu, Bochen & Davari, Pooya. (2020). Reliability of Power Electronic Systems for EV/HEV Applications. Proceedings of the IEEE. PP. 1-17. 10.1109/JPROC.2020.3031041.

[6] Conlon, B., Anwar, M., Sevel, K., Wang, M., Badawi, R., & Bavili, A. (2022). Switchable 400V/800V high voltage architecture for Ultium battery electric trucks. Proceedings of the IEEE Energy Conversion Congress and Exposition (ECCE).

[7] Ozguc, M. K., Ipek, E., Aras, K., & Erhan, K. (2019). Comprehensive analysis of pre-charge sequence in automotive battery systems. Transactions on Environment and Electrical Engineering, 4(1), 1-6.

[8] M. Braunovic, Electrical Contacts: Principles and Applications, 2nd ed., CRC Press, 2006.

[9] TE Connectivity, "EV200 Series Contactor Datasheet," [Online]. Available: https://www.te.com

[10] X. Zhang, Y. Cheng, and R. Mahajan, "Reliability and Lifetime Prediction of High Voltage Contactors for Electric Vehicle Applications," IEEE Transactions on Device and Materials Reliability, vol. 16, no. 3, pp. 357–364, Sept. 2016. DOI: 10.1109/TDMR.2016.2571732.

[11] H. S. Hwang, "Bidirectional Inverter Design with Boost Function for EV Charging and Motor Control," IEEE Transactions on Industrial Electronics, vol. 65, no. 6, pp. 4790–4798, Jun. 2018.

[12] R. W. Erickson and D. Maksimovic, Fundamentals of Power Electronics, 2nd ed., Springer, 2001.

[13] B. Jayabalan, "High-Efficiency Interleaved DC–DC Converters for EV Applications," IEEE Transactions on Industrial Electronics, vol. 68, no. 4, pp. 3324–3334, Apr. 2021.

[14] S. Dusmez and C. T. Li, "A Review of High Power Density Converters for EVs," IEEE Journal of Emerging and Selected Topics in Power Electronics, vol. 8, no. 1, pp. 626–642, Mar. 2020.

[15] F. Krismer and J. W. Kolar, "Efficiency-Optimized High-Current Dual Active Bridge Converter for Automotive Applications," IEEE Transactions on Power Electronics, vol. 24, no. 6, pp. 1480–1491, Jun. 2009.

[16] M. Borage, S. Tiwari, and S. Kotaiah, "Design and Performance Analysis of High-Current Busbars in EV Powertrains," IEEE Transactions on Components, Packaging and Manufacturing Technology, vol. 10, no. 5, pp. 945–953, May 2020.

[17] A. Boglietti et al., "Effects of Skin and Proximity Phenomena on Busbars in PWM Inverter-Fed Electric Drives," IEEE Transactions on Industry Applications, vol. 38, no. 5, pp. 1312–1318, Sep./Oct. 2002.

[18] S. Suresh, "Loss Evaluation in Laminated Busbar Structures for Power Electronic Modules," IEEE Transactions on Power Electronics, vol. 35, no. 4, pp. 3964–3973, Apr. 2020.

[19] R. Thomas, "Low Resistance Connections in High Power Systems," Journal of Electrical Engineering & Technology, vol. 14, no. 3, pp. 1297–1306, 2019.

[20] V. Smet et al., "Ageing and failure modes of IGBT modules in high-temperature power cycling," IEEE Transactions on Industrial Electronics, vol. 58, no. 10, pp. 4931–4941, Oct. 2011.

[21] Shu, X., Zhou, Q., Zhang, C., & Zhang, B. (2020). A reliability study of electric vehicle battery from the perspective of power supply system. Journal of Power Sources, 451, 227805.

[22] Ji, Y., Giangrande, P., Zhao, W., Zhang, J., & Zhang, P. (2025). Improved aging enhancement factor for reliability assessment of motor windings in electric vehicle applications. IEEE Transactions on Energy Conversion.

[23] https://uk.mer.eco/news/sweden-ev-charging-infrastructure/

[24] Uzair, M., Abbas, G., & Hosain, S. (2021). Characteristics of battery management systems of electric vehicles with consideration of the active and passive cell balancing process. World Electric Vehicle Journal, 12(3), 120.

[25] Harris, N., Shealy, T., & Klotz, L. (2017). Choice Architecture as a Way to Encourage a Whole Systems Design Perspective for More Sustainable Infrastructure. Sustainability, 9(1), 54. https://doi.org/10.3390/su9010054

[26] Capelli, F., Riba, J., & Sanllehí, J. (2017). Finite element analysis to predict temperature rise tests in high-capacity substation connectors. IET Generation, Transmission &Amp; Distribution, 11(9), 2283-2291. https://doi.org/10.1049/iet-gtd.2016.171

[27] Matthew Keyser, Ahmad Pesaran, Qibo Li, Shriram Santhanagopalan, Kandler Smith, Eric Wood, Shabbir Ahmed, Ira Bloom, Eric Dufek, Matthew Shirk, Andrew Meintz, Cory Kreuzer, Christopher Michelbacher,

Andrew Burnham, Thomas Stephens, James Francfort, Barney Carlson, Jiucai Zhang, Ram Vijayagopal, Keith Hardy, Fernando Dias, Manish Mohanpurkar, Don Scoffield, Andrew N. Jansen, Tanvir Tanim, Anthony Markel, Enabling fast charging – Battery thermal considerations, Journal of Power Sources, Volume 367, 2017, Pages 228-236, ISSN 0378-7753, https://doi.org/10.1016/j.jpowsour.2017.07.009.

[28] Moo, Chin-Sien & Ng, Kong & Hsieh, Yao-Ching. (2008). Parallel Operation of Battery Power Modules. Energy Conversion, IEEE Transactions on. 23. 701 - 707. 10.1109/TEC.2007.914310.

[29] Cao, Jian & Schofield, N. & Emadi, Ali. (2008). Battery balancing methods: A comprehensive review. Proc IEEE VPPC'. 06. 1 - 6. 10.1109/VPPC.2008.4677669.

[30] J. D. Valladolid, R. Albarado, D. Mallahuari and D. Patiño, "Experimental Performance Evaluation of Electric Vehicles (EV) Based on Analysis of Power and Torque Losses," 2020 IEEE International Conference on Industrial Technology (ICIT), Buenos Aires, Argentina, 2020, pp. 933-938, doi: 10.1109/ICIT45562.2020.9067241.

[31] https://www.kebamerica.com/blog/advantages-of-high-voltage-in-electric-vehicle-designs/

[32] I. Aretxabaleta, I. M. De Alegría, J. Andreu, I. Kortabarria and E. Robles, "High-Voltage Stations for Electric Vehicle Fast-Charging: Trends, Standards, Charging Modes and Comparison of Unity Power-Factor Rectifiers," in IEEE Access, vol. 9, pp. 102177-102194, 2021, doi: 10.1109/ACCESS.2021.3093696.

[33] Yacoub Al Shdaifat M, Zulkifli R, Sopian K, Adel Salih A. Basics, properties, and thermal issues of EV battery and battery thermal management systems: Comprehensive review. Proceedings of the Institution of Mechanical Engineers, Part D: Journal of Automobile Engineering. 2022;237(2-3):295-311. doi:10.1177/09544070221079195

[34] Omkar Mypati, Tariq Anwaar, Desham Mitra, Surjya Kanta Pal, Prakash Srirangam, Characterization and modelling of Al and Cu busbar during charging and discharging of Li-ion battery for electric vehicles, Applied Thermal Engineering, Volume 218, 2023, 119239, ISSN 1359-4311, https://doi.org/10.1016/j.applthermaleng.2022.119239

[35] A. Khaligh and S. Dusmez, "Comprehensive Topological Analysis of Conductive and Inductive Charging Solutions for Plug-In Electric Vehicles," in IEEE Transactions on Vehicular Technology, vol. 61, no. 8, pp. 3475-3489, Oct. 2012, doi: 10.1109/TVT.2012.2213104.

[36] Larminie, J., & Lowry, J. (2012). Electric vehicle technology explained. John Wiley & Sons.

[37] Cao, Jian & Emadi, Ali. (2012). A New Battery/UltraCapacitor Hybrid Energy Storage System for Electric, Hybrid, and Plug-In Hybrid Electric Vehicles. Power Electronics, IEEE Transactions on. 27. 122 - 132. 10.1109/TPEL.2011.2151206.

[38] Ehsani, Mehrdad & Gao, Yimin & Gay, Sebastien & Emadi, Ali. (2004). Modern Electric, Hybrid Electric, and Fuel Cell Vehicles: Fundamentals, Theory, and Design. 10.1201/9781420037739.

[39] Bennion, Kevin & Thornton, Matthew. (2010). Integrated vehicle thermal management for advanced vehicle propulsion technologies: Preprint.. SAE Technical Papers. 10.4271/2010-01-0836.
[40] Abraham, Thomas & Bennion, Kevin & Bharathan, Desikan & Narumanchi, Sreekant & O'Keefe, Michael. (2007). Assessment of Thermal Control Technologies for Cooling Electric Vehicle Power Electronics.
[41] Elkjær, A. S. (2024). On the Substitution of Aluminium for Copper Conductors in Battery Systems.
[42] Orazem, M. E., & Tribollet, B. (2008). Electrochemical impedance spectroscopy. New Jersey, 1(906), 383-389.
[43] Stuart, Thomas & Fang, Fang & Wang, Xiaopeng & Ashtiani, Cyrus & Pesaran, Ahmad. (2002). A Modular Battery Management System for HEVs. 10.4271/2002-01-1918.
[44] Ujah, C. O., Popoola, A. P. I., & Popoola, O. M. (2022). Review on materials applied in electric transmission conductors. Journal of Materials Science, 1-18.
[45] D. Linden and T. B. Reddy, Handbook of Batteries, McGraw-Hill, 2002.
[46] Eaton. (n.d.). Battery configuration switch. Retrieved May 30, 2025, from https://www.eaton.com/us/en-us/catalog/emobility/battery-configuration-switch
[47] International Energy Agency. (2025). Global EV Outlook 2025: Expanding sales in diverse markets. IEA. https://www.iea.org/reports/global-ev-outlook-2025

DEPARTMENT OF SPACE, EARTH, AND ENVIRONMENT
CHALMERS UNIVERSITY OF TECHNOLOGY
Gothenburg, Sweden
www.chalmers.se

CHALMERS
UNIVERSITY OF TECHNOLOGY